Journal of Marine Science and Technology

Volume 26 | Issue 3 Article 7

EVALUATION ON THE EFFICIENCY OF STABILITY REMEDIATION FOR T16-TOWER PIER SLOPE (T16-SLOPE) OF TAIPEI MAO-KONG TRAMWAY

Der-Guey Lin
Department of Soil and Water conservation, National Chung-Hsing University, Taichung, Taiwan, R.O.C.

Sheng-Hsiunng Hung
Department of Soil and Water conservation, National Chung-Hsing University, Taichung, Taiwan, R.O.C.

Wen-Tsung Liu
Department of Civil Engineering, Kao Yuan University, Kaohsiung, Taiwan, R.O.C.

Jui-Ching Chou
Department of Civil Engineering, National Chung-Hsing University, Taichung, Taiwan, R.O.C., jccchou@nchu.edu.tw

Recommended Citation

Lin, Der-Guey; Hung, Sheng-Hsiunng; Liu, Wen-Tsung; and Chou, Jui-Ching (2018) "EVALUATION ON THE EFFICIENCY OF STABILITY REMEDIATION FOR T16-TOWER PIER SLOPE (T16-SLOPE) OF TAIPEI MAO-KONG TRAMWAY," *Journal of Marine Science and Technology*: Vol. 26: Iss. 3, Article 7.
DOI: DOI: 10.6119/JMST.201806_26(3).0007
Available at: https://jmstt.ntou.edu.tw/journal/vol26/iss3/7

Journal of Marine Science and Technology, Vol. 26, No. 3, pp. 352-373 (2018)
DOI: 10.6119/JMST.2018.06_(3).0007

EVALUATION ON THE EFFICIENCY OF STABILITY REMEDIATION FOR T16-TOWER PIER SLOPE (T16-SLOPE) OF TAIPEI MAO-KONG TRAMWAY

Der-Guey Lin[1], Sheng-Hsiunng Hung[1], Wen-Tsung Liu[2], and Jui-Ching Chou[3]

Key words: finite element techniques, strength reduction method (SRM), T16-Slope, compound stabilization work, rainfall-induced seepage, stability analyses, relative factor of safety (RFS).

ABSTRACT

This study performs a series of rainfall-induced seepage and stability analyses of unsaturated slope using strength reduction method (*SRM*) of two-dimensional (2-D) finite element technique to inspect the efficiency of compound stabilization work adopted for the remediation of the down slope of *T16-tower pier* (or *T16-Slope*) situated at the hillside of Taipei City Mao-Kong tramway. The validities of numerical procedures and various material model parameters are verified by examining the triggering mechanism and occurrence time of landslide in *T16-Slope* during Jang-Mi typhoon in 2008. After the landslide in 2008, the potential sliding surfaces of *T16-Slope* with and without remediation are both developed at the up-middle-slope (the most critical sectional slope) where an *RC*-grid-beam (*RC*-grillage) and anchorage were constructed for remediation. The remediation enables to prevent the up-middle-slope from coming close to a critical state during torrential rainfall. The increasing *FS* value demonstrates the deterioration of the stability of up-middle-slope caused by groundwater rise can be mitigated by the stabilization effects of remediation. The analysis results also indicate that the stabilization effects of remediation can be greatly reduced after a rainfall with long duration and heavy intensity because of a strenuous infiltration of rainwater.

I. INTRODUCTION

In Taiwan, slope land areas are prone to landslides and always bring about disastrous soil and rock mass movements due to the inherent steep topography and fragile geological structure of natural environment. In addition, landslides in Taiwan are frequently caused by torrential rainfalls in the typhoon season and may mobilize into debris flows (Lin et al., 2008, 2009, 2012). As a consequence, massive infiltrated rainwater induced from the consecutive rainfalls and stored up in the sliding body eventually becomes a crucial factor to trigger a large scale landslide (Lin et al., 2010a, Ko and Lin, 2015). Especially, during the typhoon season, intense rainstorms often lead to a landslide and cause serious damages and injuries to the housing estate and human life. In the recent years, the devastating typhoons in Taiwan that caused large landslides, tremendous economic loss and hundreds of deaths are Typhoons Toraji on July, 30th, 2001 (111 deaths and 103 missing) and Typhoon Morakot on August, 8th, 2009 (681 deaths and 13 missing). Especially, Typhoon Morakot brought up to 2850 mm of precipitation in 100 hours to southern Taiwan and the economic loss was estimated at $912 million USD.

At approximately 20:00~21:00 p.m. on September, 28th, 2008, during Jang-Mi typhoon, a large landslide occurred at the rear slope of Royal Garden residential community in Taipei City. In this study, the slope is called *T16-Slope* because *T16-tower pier* of Taipei City Mao-Kong tramway situated at the slope top and the landslide was exactly located at the down slope of *T16-tower pier*. After the landslide occurred, due to a downward movement of soil mass during torrential rainfall, a large volume of soil loss occurred nearby *T16-tower pier*. As a consequence, due to soil loss of ground surface, a 4~5 m thick of overburden and lateral confinement was eroded from the pier shaft. Although the exposed pier shaft remained intact, the removal of lateral confinement situated the pier shaft in a cantilever length of 4~5 m above ground surface. This cantilever section may impose a large bending moment on the pier structure during earthquake. Accordingly, the safety of pier structure needs to be inspected especially for the reinforcement required to resist the design seismic loading. To prevent *T16-Slope* from jeopardizing by the recurrence of downslope failure and secure the safety of human life and residential estates at the slope toe, Taipei City Government expedited a complex remedial work to stabilize *T16-Slope* after carrying out a detailed field investigation and clarifying the structural safety of *T16-tower pier*. The prefer-

Paper submitted 11/20/17; revised 01/24/18; accepted 04/24/18. Author for correspondence: Jui-Ching Chou (e-mail: jccchou@nchu.edu.tw).
[1] Department of Soil and Water conservation, National Chung-Hsing University, Taichung, Taiwan, R.O.C.
[2] Department of Civil Engineering, Kao Yuan University, Kaohsiung, Taiwan, R.O.C.
[3] Department of Civil Engineering, National Chung-Hsing University, Taichung, Taiwan, R.O.C.

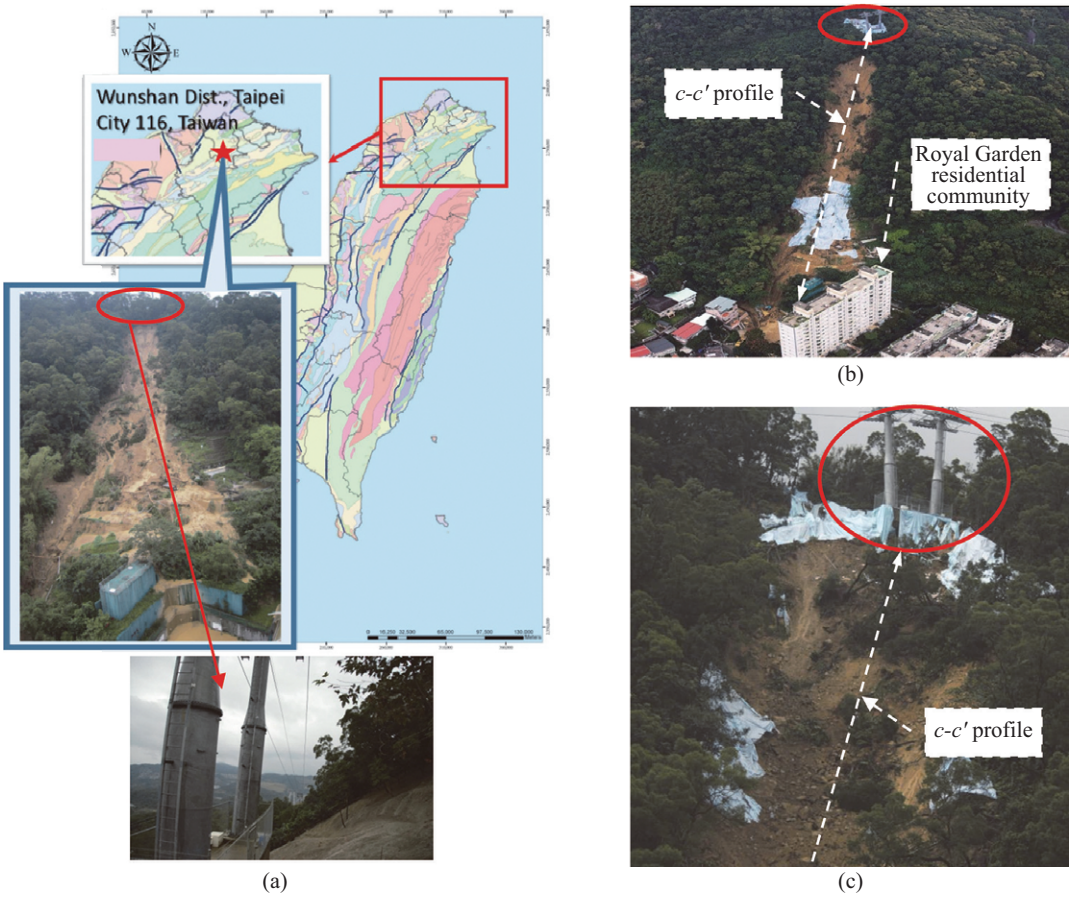

Fig. 1. (a) Location of the landslide of T16-Slope (b) Royal Garden residential community at slope toe threaten by the landslide (c) T16-tower pier of Mao-Kong tramway at slope top endangered by a downward movement of soil mass.

ential measures and optimal layout of reinforcement in different elevations of the slope had been given and discussed in the relevant technical reports (see references: Taipei City Government, 2008 and 2010).

In a homogeneous soil slope without soft band, the differences in factor of safety *FS* and locations of potential sliding surfaces (*PSS*) from the finite element strength reduction method (*SRM*) and the limit equilibrium method (*LEM*) are small and both methods are satisfactory for engineering practice (Cheng et al., 2007; Wei et al., 2009). The advantage of the *SRM* is that the *PSS* can be automatically defined by the total incremental displacement caused by the gravity loads and the strength reduction process (Berilgen, 2007; Cheng et al., 2007) and able to offer more detained information (Zheng, 2012). In addition, Bojorque et al. (2008) indicated that the *SRM* captures the different failure surfaces of multiple failure mechanisms in the entire computation steps and helps the design and the implementation of stabilization works. Retrospection to the previous simulation studies on the initiation of landslides using *SRM* (Savage et al., 2000; Debray and Savage, 2001; Chandrasekaran et al., 2013), it was rare to analyze the efficiency of stabilization works in a large landslide under rainfall-induced unsaturated seepage conditions. Instead, almost the rainfall effect in analyses was considered as a groundwater rise and consequent increase in static pore-water pressure. It should be pointed out that if the slope stability analysis was merely performed under simplified conditions without considering the real time rainfall effects on the unsaturated seepage and stability of surficial colluviums, it becomes uncertain whether the original design of stabilization works can sustain the adverse effects from infiltrated rainwater. Accordingly, this study emphasizes on identifying the effectiveness of stabilization works during torrential rainfall rather than checking their optimal layout. This study investigates the efficiency of four stabilization methods in a compound stabilization system of *T16-Slope* through transient seepage and finite element *SRM* stability analyses using PLAXIS 2D (PLAXIS 2D, 2015). The analyses also consider the unsaturated behavior of surficial colluviums under 48-hour design rainfall with different return periods.

II. LANDSLIDE OF *T16-SLOPE* IN 2008

1. Location and Topography of Landslide

T16-Slope is situated at the rear of Royal Garden residential community, Wen-Shan district, Taipei City as shown in Fig. 1. The dimension of the landslide of *T16-Slope* approximates

Table 1. Physical property of geologic strata at the landslide of *T16-Slope*.

Strata	Descriptions
SF	thickness = 2~6 m; Gravel: Sand: Silt: Clay = 0~15%:13~60%:31~70%:1~17%; γ = 17.85~19.71 kN/m^3; W_n = 8.0~19.4%; G_s = 2.67~2.71; e = 0.45~0.68; LL = 2.67~2.71%; PI = 9~10% (γ = unit weight; W_n = water content; G_s = specific gravity; e = void ratio; LL = liquid limit; PI = plastic index); USCS = *SM*, *ML*, *CL*; SPT-*N* = 15~69
SH	thickness > 20 m, a lightly weathered to fresh rock mass of grey color with low permeability
SS	massive sandstone with thickness around 16 m; contains lime material with hard material quality and high resistance to weathering and erosion; frequently appears a steep cliff landform; the rock cores exhibit a medium weathered to fresh rock mass with brown-yellow to grey-white color
SH/*ss*	Shale of grey-black color with thickness > 20 m. the rock mass contains an intercalary strata (or inter-bed) of fine sandstone; the bedrock mainly shows a fresh rock mass with grey color
SS-*SH*	Sandstone and shale alternate with thickness of about 60 m; the bedrock mainly classified as shale and locally contains an intercalary strata of sandstone and shale; the bedrock shows a lightly to medium weathered rock mass with brown-grey color

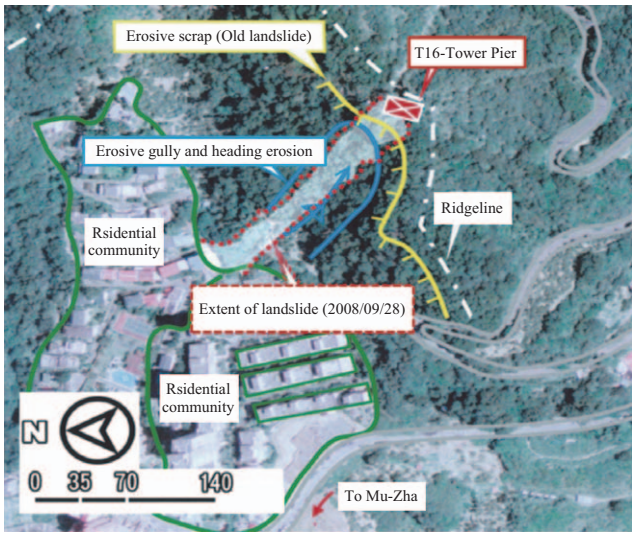

Fig. 2. Annotated aerial-photo for topographic and surface geologic interpretation on the landslide of T16-Slope.

20~80 m in width and 230 m in length and the influential area induced from slope failure comes close to 1.17 hectares (117,00 m^2). The total volume of the sliding soil mass is estimated about 30,000 m^3. The elevation of the landslide ranges from 280 to 150 m and the topographic elevation descends from southeast to northwest.

The top of landslide (Fig. 2, red dotted line) of *T16-Slope* possesses an elevation about 274.5 m and an average gradient of 58% in 2008. The topography of landslide appears a hill-concave landform and prone to accumulate run-off during rainfall. As a consequence, the rock strata in this area are liable to weathering and heading erosion. A *C*-*C*′ profile crossing over the central region of *T16-Slope* was adopted for a series of rainfall-induced seepage and slope stability analyses as shown in Fig. 1(b). Using the annotated aerial photograph of *T16-Slope*, as illustrated in Fig. 2, one can interpret the characteristics of watershed, basin, terrace distribution, possible soil strata and soil erosion in the slope. At the northern area (left side or downward area of the scarp) of ridgeline (Fig. 2, white dotted line), the vegetation grows dense with leaves and presents deep green color. It can be deduced that the area possesses a thicker soil stratum and plenty of groundwater at all seasons.

On the other hand, at the southern area (right side or area with gentle gradient) of ridgeline, in addition to cultivation plants, the growth of vegetation is influenced by seasons and the vegetation grows loose with light green to light brown color. This indicates that the area has thinner soil stratum and thicker bedrock with high permeability which alternately leads to a lower groundwater table in dry season. In addition, the aerial photograph also illustrates a scarp of bow shape at the down slope of *T16-tower pier* (Fig. 2, yellow solid line) and it is speculated as the top fringe of old landslide. Further on, at the down slope area of the top fringe, the topography displays a concave channel of arc shape and it is conjectured as a geological feature resulted from shallow landslide of rotational sliding. Conclusively, based on the entire pattern of concave channel, the channel can be classified as an erosive gully caused by heading erosion (Fig. 2, light blue solid line).

2. Geology of *T16-Slope*

According to the field investigations, the outcrop of landslide can be classified as Da-Liao formation and consisted of sandstone (*SS*), grey/black shale (*SH*), and silty sandstone with fine to medium grain particle. From 6 outcrops and 14 boreholes, the bedding plane of bedrock of *T16-Slope* demonstrates a strike of 50°N~60°E and a dip of 10°~20°SE. *T16-Slope* can be categorized as a monocline with an inclination to southeast in geologic structure and an anaclinal slope in geology. In addition, from borehole data, the surface overburden layer has a thickness of 2~6 m. The soil profile of *T16-Slope* is shown in Fig. 7(a).

One 115 m long and 50 m deep resistivity survey line and one 115 m long seismic refraction survey line (both parallel to *C*-*C*′ profile in Fig. 1(c)) were performed to investigate the geological structure of *T16-Slope*. According to the electricity resistivity and *P*-wave velocity profiles, the topography and geologic profile of *T16-Slope* can be simplified into five layers from shallows to depths as: surficial colluviums (*SF*), shale (*SH*), massive

Table 2. Material model parameters for various soil strata.

Stratum	Colluviums (*SF*)	Sandstone (*SS*)	Shale (*SH*)	Shale with inter-bed of sandstone (*SH*/*ss*)	Sandstone and shale alternate (*SS*-*SH*)
e	0.616	0.150	0.140	0.148	0.145
γ_{unsat} (kN/m^3)	19.5	24.6	23.6	23.8	24.2
γ_{sat} (kN/m^3)	20.1	25.4	24.6	24.9	25.0
ν'	0.30	0.25	0.27	0.26	0.26
c' (kPa)	5.0	680.0	256.0	306.0	468.0
ϕ'(°)	26	36	27	30	32
k_x, k_y (=k_{sat})(cm/sec)	8.08×10^{-3}	10^{-9}	10^{-9}	10^{-9}	10^{-9}
E'(kPa)	1.40×10^{4}	1.78×10^{6}	4.91×10^{5}	8.76×10^{5}	1.14×10^{6}
Remarks: e = void ratio; γ_{unsat} = unsaturated unit weight; γ_{sat} = saturated unit weight; ν' = Poisson's ratio; E' = Young's modulus; c' = cohesion; ϕ' = friction angle; k_{sat} = saturated permeability. ψ = dilatancy angle = 0.0 (ψ is taken to be zero for all strata)					

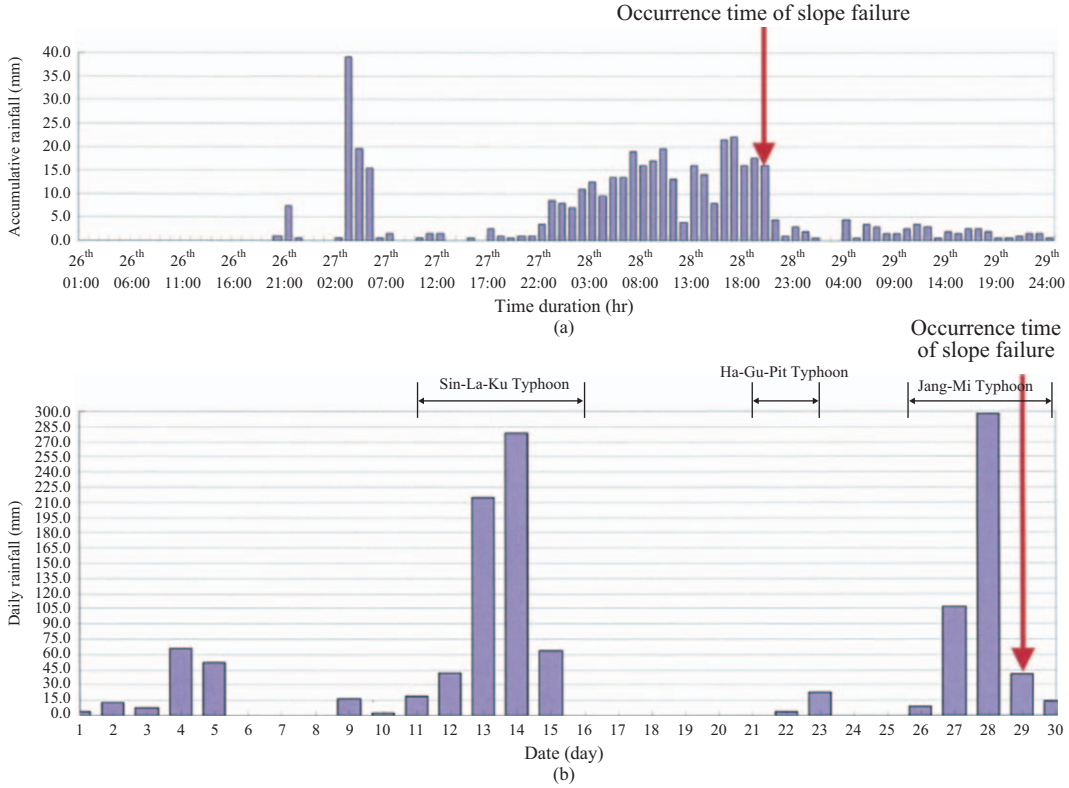

Fig. 3. (a) Hourly rainfall hyetograph (9/26~9/29, 2008 with total rainfall duration of 77 hours) during Jang-Mi typhoon (b) Daily rainfall hyetograph of September, 2008.

sandstone (*SS*); shale with an intercalary sandstone stratum (or inter-bed) (*SH*/*ss*); and sandstone/shale alternate (*SS*-*SH*). The physical properties of the five geologic materials are summarized in Table 1.

3. Rainfall Analyses for the Landslide of *T16-Slope* during Jang-Mi Typhoon in 2008

According to the records of *CWB* (Central Weather Bureau), the alert duration of Jang-Mi typhoon, which causes the landslide of *T16-Slope*, was from 26th to 29th September, 2008. The Mu-Zha rain-gauge station of *CWB* nearby the landslide indicates that the total rainfall in the alert duration of the typhoon approximates 453.0 mm. Meanwhile, the rainfall starts from 8:00 a.m., 9/26, 2008 and lasts 64 hours till the occurrence of landslide during 20:00~21:00 p.m. The cumulative rainfall for the 64 hours is 406.5 mm and which accounts for 89.74% of the total rainfall during Jang-Mi typhoon (9/26~9/30, 2008) and a maximum daily rainfall 297.5 mm/day occurs on 9/28.

Fig. 3(a) exhibits the hourly rainfall hyetograph during Jang-Mi typhoon (rainfall duration of 77 hours) and it also indicates

the landslide of *T16-Slope* occurs at the 64th hour. In addition, the daily rainfall records during September, 2008 from Mu-Zha rain-gauge station of *CWB* indicate that Sin-La-Ku (9/11~9/16, 2008), Ha-Gu-Pit (9/21~9/23, 2008) and Jang-Mi (9/26~9/30, 2008) typhoons invaded north Taiwan and accompanied with an accumulated rainfall of 1271.5 mm as shown in Fig. 3(b). The influence of these typhoons in September, 2008 on the occurrence of landslide of *T16-Slope* could be enormous. The consecutive heavy rainfalls may increase the water content and lead to a long-term fully saturated condition of soil mass. Consequently, thes typhoons could cause several extremely adverse situations to the soil mass such as material softening, increase of unit weight, and decrease of shear strength.

Several simulations (Tsaparas et al., 2002) indicated that saturated coefficients of permeability k_{sat} significantly controls the infiltration process in the slope. Nevertheless, the highly permeable soil slopes ($k_{sat} = 10^{-4}$ m/sec), are unlikely to be influenced by small amounts of antecedent rainfall. The infiltration process during a major rainfall event can be affected by antecedent rainfall if a slope is composed of a moderately permeable soil ($k_{sat} = 10^{-5}$ m/sec). Further on, several researchers (Collins and Znidarcic, 2004; Rahardjo et al., 2007; Singh et al., 2013) also indicated that the effect of antecedent moisture conditions can considerably affect slope stability. In *T16-Slope*, the saturated coefficient of permeability of surficial colluviums $k_{sat} = 8.08 \times 10^{-5}$ m/sec (see Table 2) is greater than 10^{-5} m/sec and approximates 10^{-4} m/sec. The surficial colluviums can be classified into a highly permeable soil stratum and are unlikely to be influenced by small amount of antecedent rainfall. The effect of antecedent rainfall from two earlier typhoons can be neglected due to the smaller amount of rainfall during Ha-Gu-Pit typhoon and the longer time interval (more than 2 weeks or 14 days) of Sin-La-Ku typhoon to the main rainfall event Jang-Mi typhoon (Fig. 3(b)). Because the potential sliding surfaces are mainly initiated in surficial colluviums, the associated rainfall-induced seepage and slope stability analyses are then designed to perform in top surficial layer numerically. To achieve above analyses, a smaller and identical value of hydraulic conductivity 10^{-9} cm/sec (Table 2) for bedrocks is then assigned in the numerical model. Conclusively, determination of the unsaturated hydraulic conductivity of surficial colluviums properly should be the most essential issue to the entire numerical modeling.

4. Remediation of Landslide

After the landslide, Taipei City Government immediately launched a field investigation together with project managers, designers, and contractors of Taipei Mao-Kong Tramway engineering project. On 29th September, 2008, the date of landslide, a temporary drainage-way was installed at the toe area of *T16-Slope*, as shown in Fig. 4(a), to divert the run-off into an existing drainage ditch at downslope and secure the safety of Royal Garden residential community below the toe area. Simultaneously, various urgent countermeasures at the toe area of *T16-Slope* were constructed from the next day (9/30, 2008), as presented in Figs. 4(a) and (b). The countermeasures consist of: (1) installation of temporary run-off detention and silt sedimentation pools, (2) stacking soil bags and piling of steel rail to retain sliding soil and rock debris, (3) spreading out of plastic canvas cover on the landslide to mitigate the erosion of run-off.

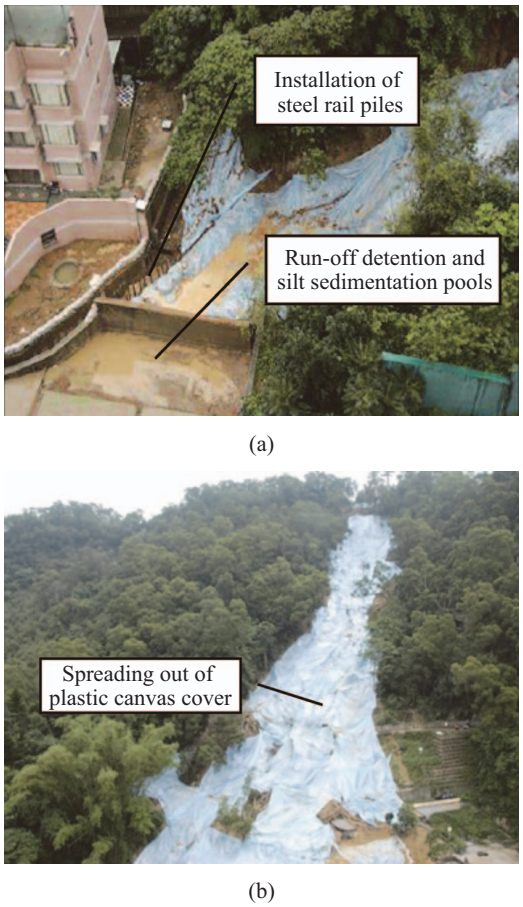

Fig. 4. Temporary emergency countermeasures after the landslide of T16-Slope (a) construction of run-off detention and silt sedimentation pools, stacking of soil bag and installation of steel rail pile (b) laying plastic canvas cover.

Considering the topographic and geologic conditions, and the triggering mechanism of landslide, Taipei City Government initiated a series of engineering designs for permanent remediation. In addition to the fragility of geologic structure, the landslide of *T16-Slope* was mainly resulted from the run-off and the concurrent ground surface erosion during extremely heavy rainfall. As a consequence, the engineering designs of remediation should take the slope stabilization, surface drainage improvement, and green plants beautification into account. Due to the strategic importance of the *T16-Slope*, the design and construction of remedial works were quickly implemented prior to the next typhoon when further detrimental ground movements would be inevitable.

The major permanent remediation included: (1) slope stabilization facilities (micro-pile, retaining wall, and retaining pile), (2) slope protection facilities (*RC*-grid-beam or *RC*-grillage and anchorage, *RC*-frame with soil nailing), (3) run-off interception

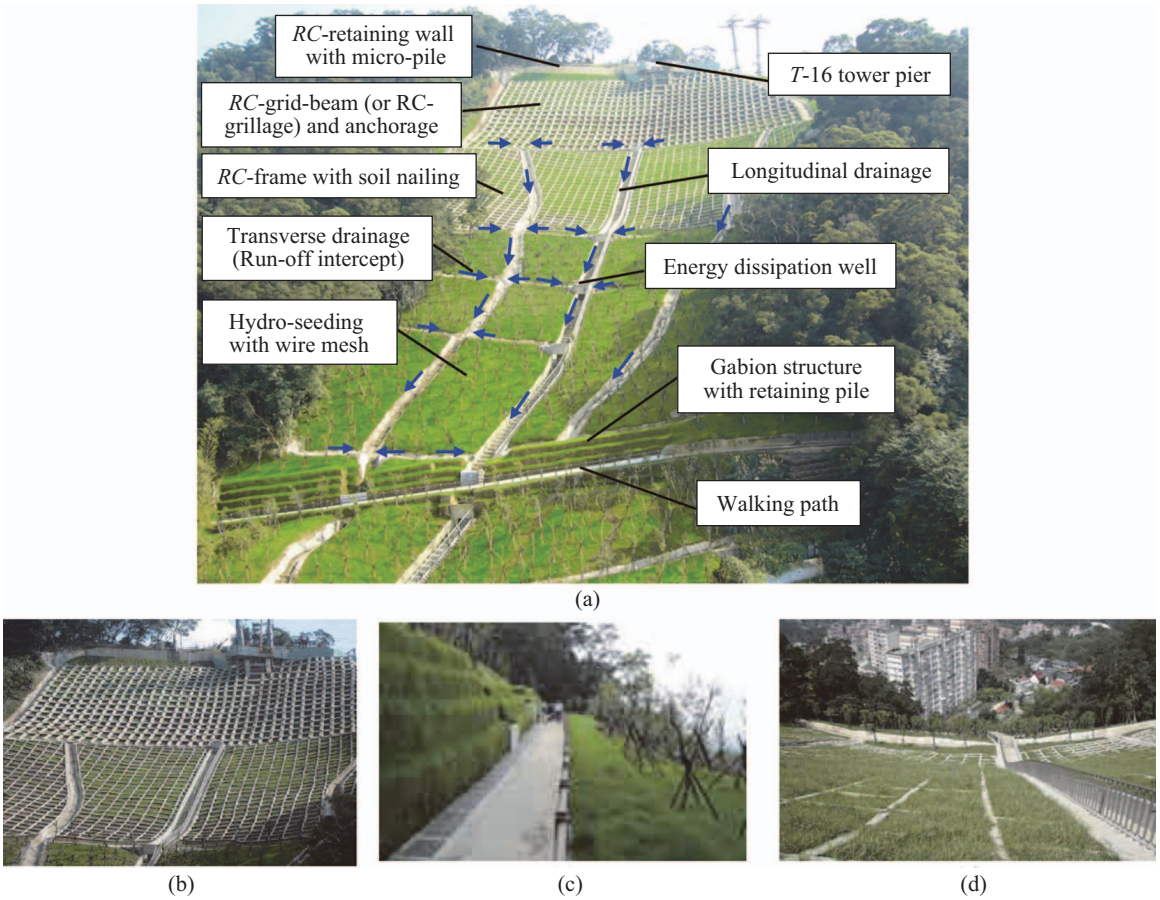

Fig. 5. (a) Overall configuration of remediation in T16-Slope (b) *RC*-grid-beam (or *RC*-grillage) and anchorage at up-middle-slope and *RC*-frame with soil nailing at middle-slope (c) Gabion structure and walking path with retaining piles at down-slope (d) A bird's-eye view from *RC*-frame with soil nailing and hydro-seeding at middle-slope.

and drainage facilities (horizontal and longitudinal surface drainage or run-off interceptor), (4) greening and vegetation. These remedial works were originally designed based on the official design criteria with engineering practices and identified by the slope stability analyses of the conventional limit equilibrium method. However, the stability evaluation excluded the effect of the rainwater infiltration on the unsaturated surficial colluviums during the torrential rainfall and which is investigated in this study to verify the performances of various remedial works under 48 hours design rainfall of different return periods. The main purposes of the remediation are aimed to intercept and drain run-off safely, improve the slope stability and beautify the environment with the plant greening and vegetation. The remediation was completed one after another from February to August, 2010. Fig. 5 illustrates the completed remediation in *T16-Slope* and which can be detailed as follows:

1. Steel rail reinforced micro-piles and *RC*-retaining wall (up-slope remediation at an elevation of 280~270 m): to stabilize soil mass at slope top. To avoid the sliding of soil mass which endangers the safety of construction at down-slope, there were totally 503 micro-piles (40-Nkg steel rail, spacing of 0.8 m, diameter of 25 cm) installed at the upslope of *T16*-tower pier.
2. *RC*-grid-beam (or *RC*-grillage) and anchorage and hydro-seeding (up-middle-slope remediation at an elevation of 270~240 m): to stabilize steep, thick and jointed sandstone slope. Due to the steep topography and exposed fragmented bedrock, a higher resistance to stabilize the slope is necessary. There were totally 617 anchors (total length of 25 m, anchorage length of 10 m, pre-stress of 40 tons, horizontal and vertical spacing of 2 m, and elevation angle of 30° to horizontal) mounted on *RC*-grid-beam (grid size: 2 m × 2 m, beam cross section: width × depth = 50 cm × 65 cm) to stabilize the slope surface with an area about 4,055 m^2.
3. *RC*-frame with soil nailing and hydro-seeding (middle-slope remediation at an elevation of 240~215 m): to stabilize the slope by increasing the stiffness of soil strata. Without exposed bedrock, the middle-slope has a milder inclination and thicker overburden. As a consequence, the required resistance for slope stabilization is lower than that of up-middle-slope. There were totally 1,130 soil nailing (length of 6 m, horizontal and vertical spacing of 2 m, and elevation angle of 25° to horizontal) mounted on *RC*-frame (frame size: 2 m × 2 m,

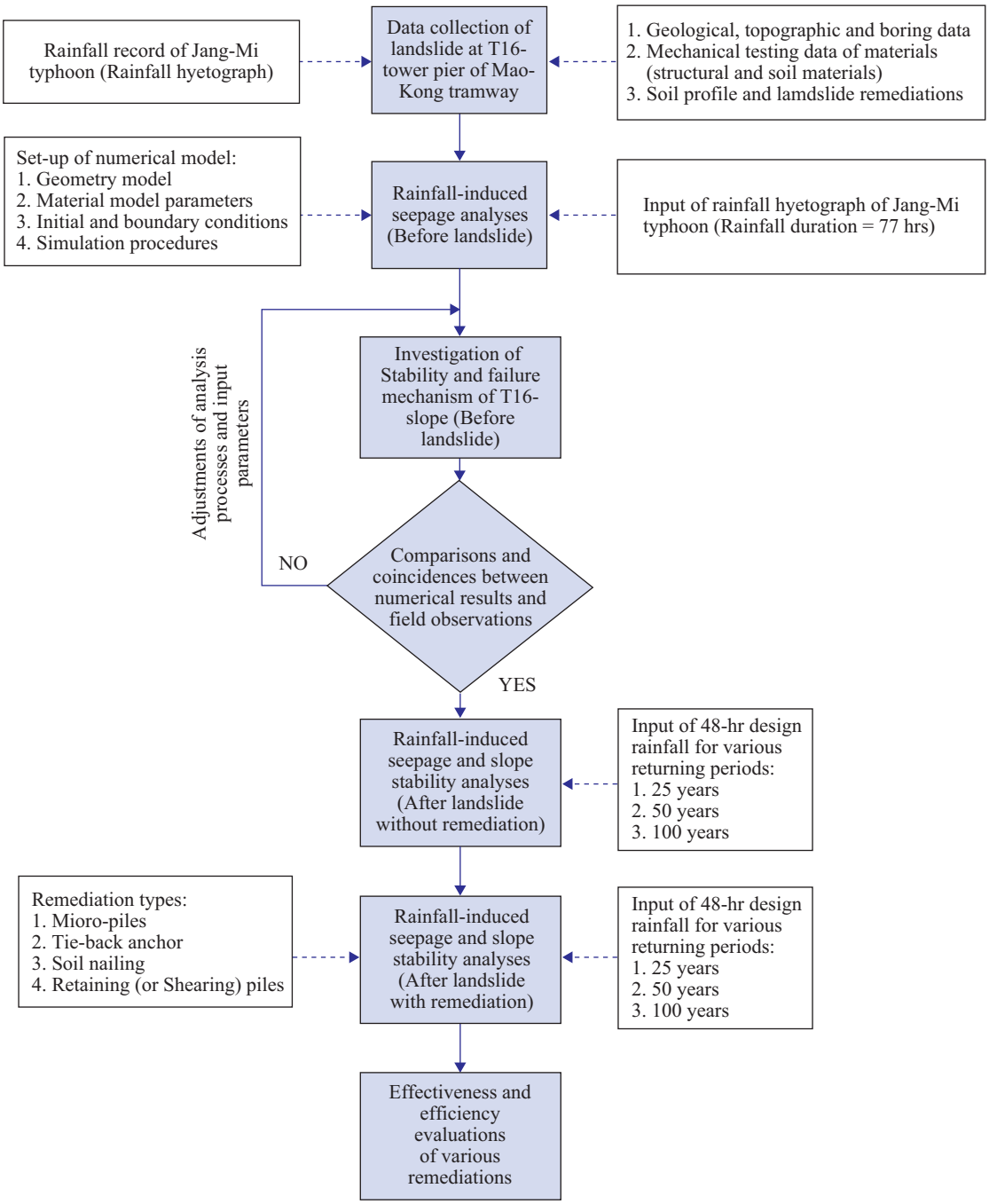

Fig. 6. Framework and flowchart of the study.

frame cross section: width × depth = 20 cm × 20 cm) to stabilize the slope surface with an area about 3,645 m^2. In addition, the slope surface was greening by hydro-seeding.

4. Retaining piles and gabion structure (down-slope remediation at an elevation of 203~180 m): to stabilize the overburden and restore the walking path. Similarly, the down-slope possesses a gentle inclination and thicker overburden. To prevent the slope from deep-seated sliding failure, three rows of 104 retaining piles (diameter of 80 cm, length of 15 m, and spacing of 1.2 m) were installed and the pile tops were connected by a pile cap to enhance the structural integrity and overall stiffness of pile group.
5. Hydro-seeding with wire mesh and vegetation (slope toe remediation at an elevation lower than 215 m): to prevent the bared area from run-off erosion. To avoid further surface erosion during rainfall, a large area of hydro-seeding with placement of wire mesh and vegetation restoration were carried out on the bared land at slope toe. In addition, there were totally 710 Taiwan golden-rain trees and alder trees planted to protect the slope surface against soil erosion.

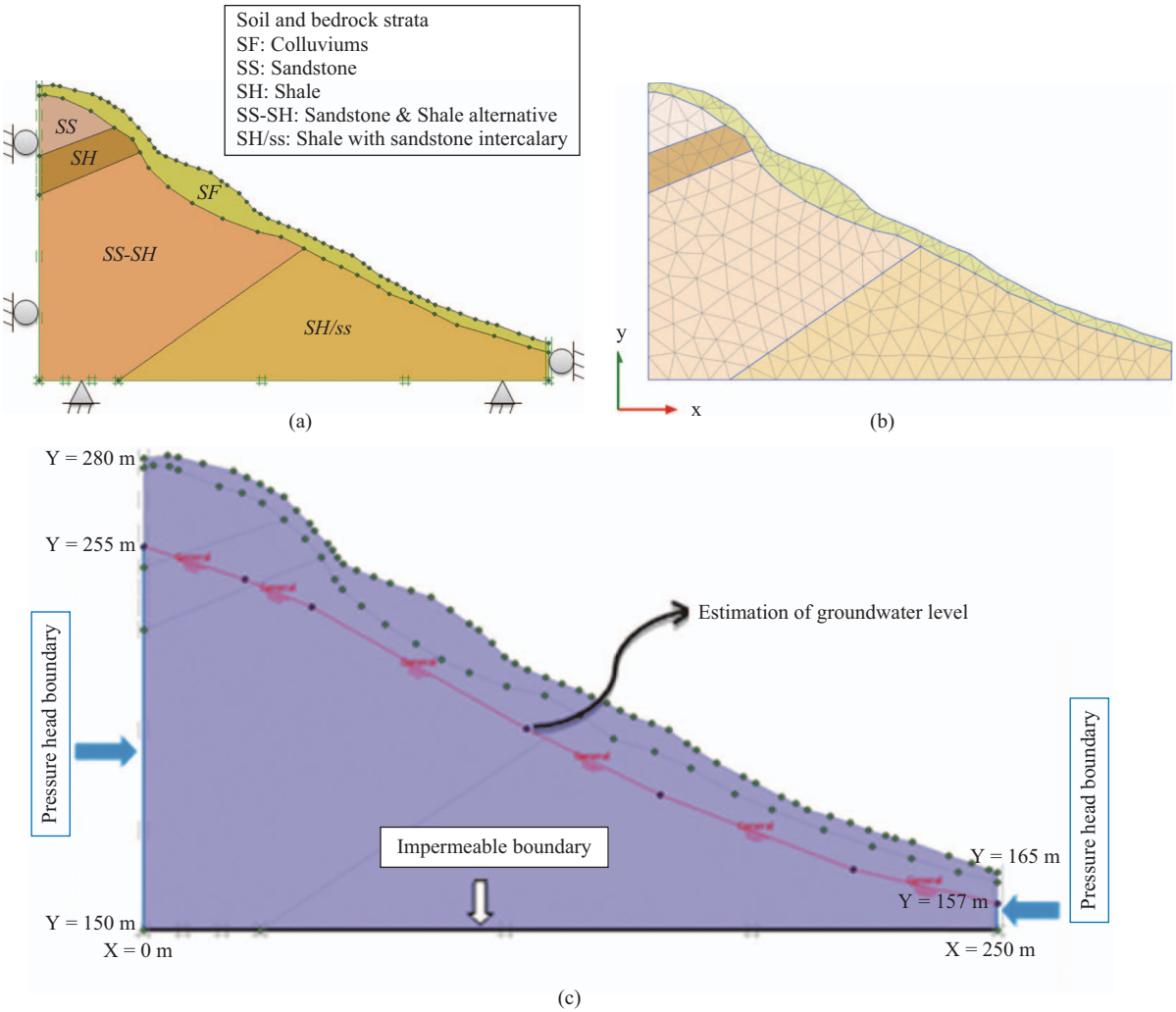

Fig. 7. (a) Numerical model with displacement B.C. (b) Finite element mesh (c) Initial groundwater level of T16-Slope in 2006 before landslide.

6. Intercept and drainage systems (from middle-slope to slope toe): to drain off the run-off during heavy rainfall, longitudinal and transverse drainage ditches with total length of 193 m, 8 sets of energy dissipation wells, and 1 set of detention and silt sedimentation pool were constructed. The run-off was collected by transverse drainage (intercept ditch) and accumulated to longitudinal drainage (drainage ditch). Rainwater flows along the longitudinal drainage through 8 sets of energy dissipation wells and drains into detention and silt sedimentation pool at the end of slope toe. Eventually, the run-off was drained away safely to the existing external drainage system.

III. METHODS AND MATERIALS

1. Flow Chart and Framework of the Study

The framework and flowchart of the study are illustrated as Fig. 6. This study is aimed at investigating the triggering mechanism of landslide and the efficiency of remedial works in *T16-Slope*. The landslide location and occurrence time of numerical results are compared with those of field observations to verify the validities of input material model parameters and numerical procedures.

2. Seepage and Stability Analyses of Rainfall-Induced Landslide in *T16-Slope* During Jang-Mi Typhoon

Using the rainfall hyetograph of Jang-Mi typhoon in 2008, a numerical simulation of rainfall-induced slope failure was performed in the duration of rainfall. During Jang-Mi typhoon, the rainfall started from 09/26, 8:00 a.m. till 09/28 20:00~21:00 p.m. when the landslide occurred. The effectiveness of numerical procedures and input material model parameters can be verified by inspecting the coincidence between simulations and observations of the post-failure topography, landslide location, and landslide occurrence time in *T16-Slope*.

The numerical model is shown in Fig. 7. The material model parameters of soil strata are primary determined by the general tests of physical properties, unconfined compression tests and direct shear tests of undisturbed samples (Taipei City Government, 2008) and calibrated by the landslide event of Jang-Mi

Table 3. Material parameters for the hydraulic conductivity of unsaturated overburden colluviums of T16-Slope.

Soil classification method	*USDA*	
Soil type	Silty Loam: *SM*/*CL*/*ML*	
Distribution of soil particle size	Particle size (μm)	Content (%)
	< 2.0	14
	2.0 ~ 50.0	65
	> 50.0	21
Hydraulic conductivity model of unsaturated soil		*vG*-model
Saturated hydraulic conductivity k_{sat} (= k_x = k_y)		0.2984 (m/hours) or 8.08×10^{-3} (cm/sec)

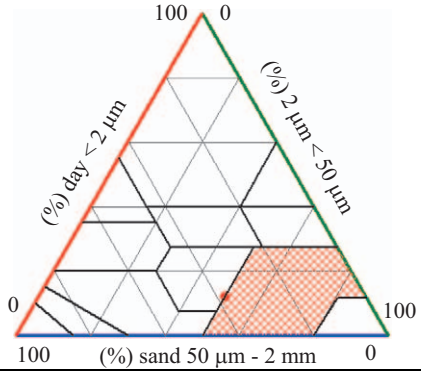

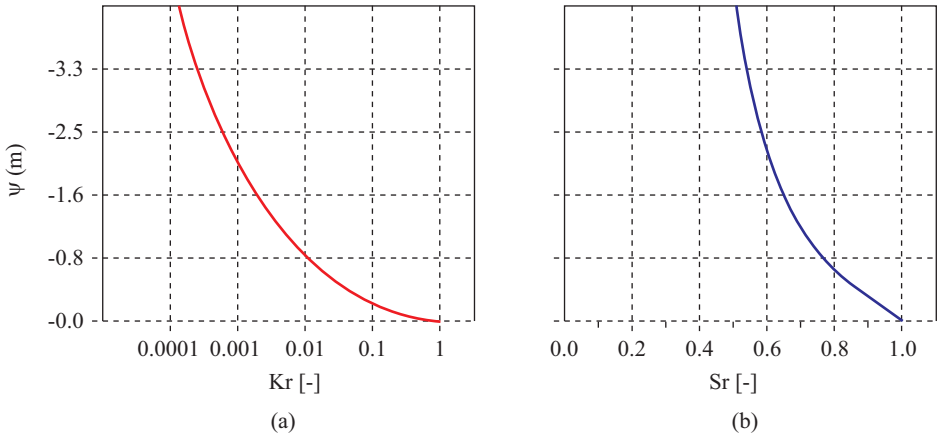

Fig. 8. (a) Hydraulic conductivity curve kr(Ψ)~Ψ (b) saturation degree curve Sr(Ψ)~Ψ of vG-model for unsaturated overburden colluviums of T16-Slope.

typhoon through inspecting the coincidence between simulations and observations of the post-failure topography, landslide location, and landslide occurrence time in *T16-Slope*. In stability analyses of SRM, the Mohr-Coulomb constitutive model was used and the required material model parameters are listed in Table 2.

According to the pore pressure measurement, the surficial colluviums (or overburden colluviums) and the underlain fragmented bed rock constantly situates above the groundwater level in dry season under unsaturated condition. A tensionmeter (or tensiometer) was used for the direct measurement of negative pore-water pressure u_w and which is numerically equal to the matric suction ($u_a - u_w$) when the pore-air pressure u_a is atmospheric (i.e., u_a = zero gauge pressure = 0, ($u_a - u_w$) = u_w). The field measurements indicate that the initial matric suction u_w (= $\psi \times \gamma_w$; ψ=negative pressure head) of surficial colluviums within a depth of 0.3~1.5 m in dry season is in a range of -8.0 ~ -70.0 kPa (or matric suction head of -0.8~-7.0 m). However the matric suction of unsaturated surficial colluviums can be eliminated by the rainwater infiltration during rainfall and which alternately becomes a basis of evaluating the potential of rainfall-induced landslide (Fredlund and Rahardjo, 1993).

The required saturated hydraulic conductivity of surficial colluviums k_{sat} (= k_x = k_y = 10^{-4}~10^{-5} cm/sec) in 2-D finite element seepage analysis was determined by in-situ Guelph infiltration test. The testing results are coincident with the permeability of most overburden colluviums being classified as clayey soil (*CL*) or silty soil (*ML*) with low plasticity. The technical properties of unsaturated soil can be obtained through empirical approach based on the basic physical properties of the soil (Fredlund and Morgenstern, 1997). In this study, the required unsaturated hydraulic conductivity k_{unsat} (ψ) and relative permeability coefficient curve k_r (ψ)~ψ (or Hydraulic Conductivity Function, *HCF*), in which, k_r (ψ) = (k_{unsat} (ψ)/k_{sat}) ≤ 1.0 (ψ = negative pressure head = matric suction head), can be determined by *USDA* soil classification method, grain size distribution and *vG* hydraulic conductivity model or *vG*-model (van Genuchten, 1980) for unsaturated surficial colluviums as shown in Table 3. The k_r (ψ)~ψ curve and associated relative saturation degree curve S_r (ψ)~ψ are illustrated in Figs. 8(a) and (b) respectively. (S_r (ψ) = S_{unsat} (ψ)/S_{sat}; in which, S_{unsat} (ψ) and S_{sat} are unsaturated and saturated degree of saturation). The unsaturated hydraulic conductivity is crucial to the calculation of degree of saturation (or wetting front) and the mobilization of potential sliding surface in surficial colluviums. Incorporating the field measurements of

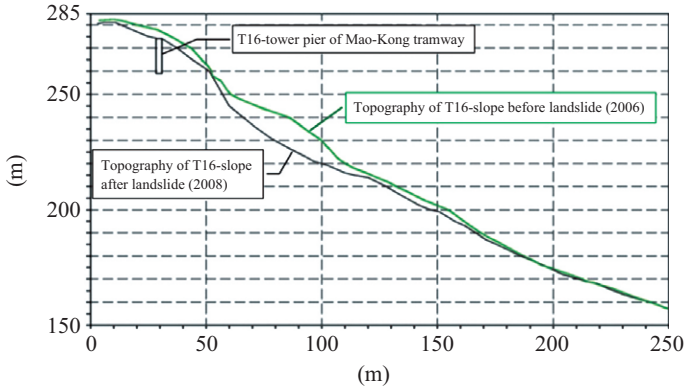

Fig. 9. Topography of C-C′ profile of T16-Slope before (2006) and after (2008) landslide.

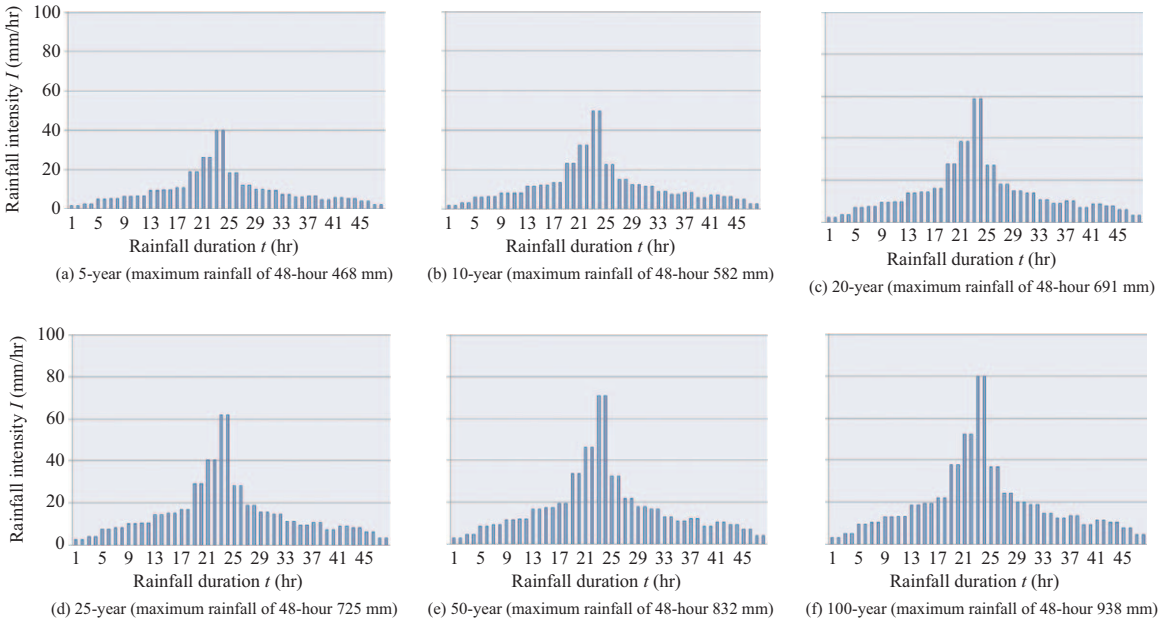

Fig. 10. 48-hour design rainfalls (or rainfall hyetographs) for different return periods.

matric suction (uw = -8.0~-70.0 kPa) with the saturated parameter k_{sat}, an unsaturated hydraulic conductivity function kr can be specified for a range of matric suction head of -0.8~-4.1 m (Fig. 8) to model the unsaturated seepage behaviors of surficial colluviums properly.

This study performs a finite element transient seepage analysis on *T16-Slope* using hourly rainfall hyetograph of Jang-Mi typhoon (9/26~9/29, 2008) with rainfall duration t = 77 hours as shown in Fig. 3(a). The time-dependent pore pressures of soil mass are determined by the transient seepage analysis and which alternately adopted for a stability analysis of *SRM* to inspect the triggering mechanism of landslide in *T16-Slope* during typhoon. In the stability analyses, the time-dependent factor of safety $FS(t)$ of *T16-Slope* is calculated for each time increment Δt (= 8 hours) for a rainfall duration t (= 0 → 77 hours).

A $FS(t) < 1.0$ means that the slope is at failure and it was agreed that a factor of safety of 1.5 is required to meet long term stability of remedial works (Hoek, 2006). In Taiwan, three *FS* values are adopted as technical criteria for slope engineering design: (1) for ordinary time $FS \geq 1.5$, (2) for earthquake $FS \geq 1.2$, (3) for torrential rainfall $FS \geq 1.1$. Moreover, Popescu (2001) proposed a three-stage continuous spectrum of *FS* to define the stability state of slopes: $FS > 1.3$ (stable), $1.0 < FS < 1.3$ (marginally stable), and $FS < 1.0$ (actively unstable).

Subsequently, the numerical results of landslide location and occurrence time are compared with field observations, namely, the location of potential sliding surface and a rainfall duration t for the critical state of $FS(t) \approx 1.0$ are inspected to verify the rationality of input material model parameters and numerical procedures. Fig. 3(a) indicates the occurrence time of landslide approximates at the 64th hour of rainfall duration. The variation of topographic elevation and failure mode of *T16-Slope* before (2006) and after (2008) landslide, namely, the pre- and post-failure slope configurations are displayed in Fig. 9.

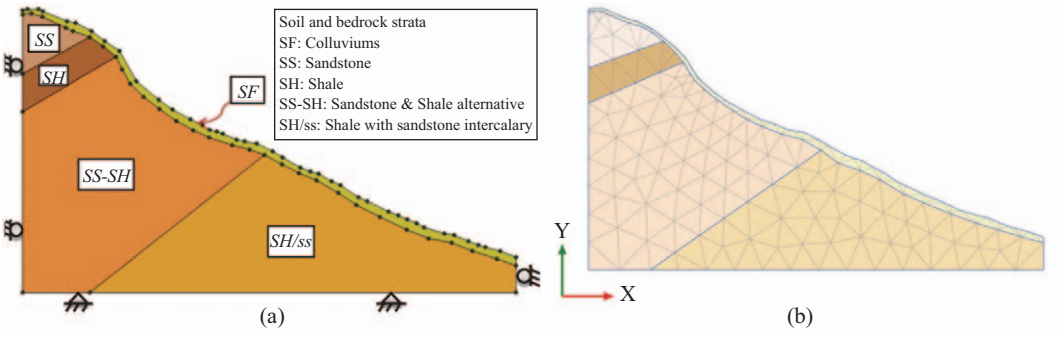

Fig. 11. (a) Numerical model (b) finite element mesh of T16-Slope after landslide without remediation in 2008.

3. Frequency Analysis of Design Rainfall Analysis

This study carried out a series of frequency and pattern analyses for the specific rainfall of landslide area using 20 years' (1989~2008) rainfall records from Mu-Zha rain-gauge station of *CWB* adjacent to the *T16-Slope*. The torrential rainfall during typhoon always displays a central-peak (or single-peak) rainfall pattern rather than the post-peak or multi-peak patterns. Incorporating the rainfall distribution percentage of the central peak into rainfall frequency analyses, the design rainfalls can be determined. Finally, the rainfall-induced seepage analyses were performed under a 48-hour design rainfall of 5-, 10-, 25-, 50- and 100-year return periods as shown in Fig. 10.

4. Rainfall-Induced Seepage and Stability of *T16-Slope* after Landslide without Remediation

In this section, analyses were carried out to inspect the possible adverse consequences of the slope as the remediation remaining not available using the *C-C′* profile of *T16-Slope* after landslide.

As shown in Fig. 11, the numerical model was fabricated according to the C-C′ profile of *T16-Slope* after landslide during Jang-Mi typhoon and without remediation. The material model parameters for various strata calibrated by landslide event of Jang-Mi typhoon were used (Table 2). Rainfall-seepage analyses using the rainfall hyetographs with return periods of 5-, 10-, 25-, 50- and 100-year (Fig. 10) were performed to capture the variations of pore-water pressure and stability in soil mass during rainfalls. However, it should be pointed out that the *T16-Slope* after landslide without remediation fails to maintain stable under a rainfall with return period of 100-year. In stability analysis, each analysis was carried out for a time increment of Δt (= 6 hours) to calculate the time-dependent factor of safety $FS(t)$ of *T16-Slope*.

5. Rainfall-Induced Seepage and Stability of *T16-Slope* after Landslide with Remediation

In the remediation works of *T16-Slope*, a large area of hydro-seeding was implemented for the plant growth to protect the slope surface from run-off erosion and promote the slope stability using vegetation root. The reinforcement effect of vegetation root on the slope stability has been widely investigated by many researchers (Frydman, 2002; Wu et al., 2004; Operstein and Lin et al., 2007). In summary, the reinforcement effect of vegetation root can be considered by adding a group of root inclusions into the soil mass or using an equivalent reinforced layer with additional cohesion increment (or shear strength increment) to represent the soil-root layer (Lin et al., 2010b). Typical values of the increase in soil cohesion due to roots range from 1.0 to 17.5 kPa (O′Loughlin and Ziemer, 1982). However, it should be mentioned that the reinforcement effect of the vegetation root on the slope stability due to hydro-seeding was not included in the numerical simulation.

The numerical model of *T16-Slope* after landslide with remediation is constructed according to the topography of *T16-Slope* after landslide (Figs. 9 and 11) and the detail design drawing of permanent remediation provided by Taipei City Government (Taipei City Government, 2010) as displayed in Fig. 12. In numerical model, *T16-Slope* can be partitioned into 4 sectional slopes with different remediation methods from slope top to slope toe (Fig. 12(a)) and which consist of (1) Up-slope: micropile of steel rail and *RC*-retaining wall, (2) Up-middle-slope: *RC*-grid-beam and anchorage, (3) Middle-slope: *RC*-frame with soil nailing, (4) Down-slope: retaining piles. The boundary conditions and mesh generation are similar to those of Fig. 11. In 2-D plane strain analysis of finite element method (FEM), various structural elements introduced to simulate the engineering structures in remediation should consider the effect of spacing S_z in the normal-direction (or z-axis) on the strength parameters of axial stiffness EA and flexural stiffness EI. The strength parameters determined according to the detail drawing of engineering design (Taipei City Government, 2008) are adjusted by multiplying an adjustment coefficient of $(1/S_z)$ as summarized in Table 4. In addition, a zero thickness interface element with relatively high normal stiffness and low shear stiffness is introduced to simulate the relative displacement and interaction behaviors of soil/structure interface.

According to Fig. 10, 48-hour rainfall hyetographs of 5-, 10-, 25-, 50- and 100-year return period were adopted for a series of rainfall-induced seepage and stability analyses. Stability analyses using *SRM* were performed for the entire *T16-Slope* with a time increment of 6 hours (= Δt). The time-dependent factor

Table 4. Material model parameters for various engineering structures of remediation.

Engineering structure		Length L (m)	Cross sectional area A ($\times 10^{-3}$ m^2)	Configuration spacing along unity width in z-axis S_z (m)	Elastic modulus E_c or E_s (kN/m^2)	Adjusted axial stiffness $(EA)_{adjusted}$ (kN/m)	Adjusted flexural stiffness $(EI)_{adjusted}$ (kN/m^2/m)	Poisson's ratio ν'
Micro-pile		8.5~12.5	4.53	0.8	2.15×10^6	1.22×10^4	4.40	0.2
Anchor	Free section	15.0	31.4	2.0	2.00×10^8	3.14×10^6	-	--
	Grout section	10.0	94.4	2.0	2.15×10^6	2.03×10^5	-	--
Soil nailing		6.0	40.0	2.0	1.97×10^6	3.94×10^4	2.82×10^1	0.2
Retaining pile		15.8	503.0	1.2	2.15×10^6	9.01×10^5	2.98×10^4	0.2
RC-retaining wall: unit weight $\gamma_{unsat} = \gamma_{sat} = 23.54$ (kN/m^3), elastic modulus $E_c = 2.15 \times 10^6$ (kN/m^2), cohesion $c' = 100$ (kN/m^2), friction angle $\phi = 45°$, permeability $k_x = k_y = 2.5 \times 10^{-5}$ (m/hours), Poisson's ratio $\nu' = 0.2$								
Remarks: Elastic modulus of steel bar (reinforcement) $E_s = 2.04 \times 10^6$ (kg/cm^2) $= 2.00 \times 10^8$ (kN/m^2) Elastic modulus of concrete $E_c = 1.50 \times 10^4 (f_c')^{0.5}$ (kg/cm^2) $= 1.47 \times 10^6 (f_c')^{0.5}$ (kN/m^2) f_c'=compression strength of concrete=175 or 210 (kg/cm^2) Unit weight of pure concrete=2300 (kg/m^3)=22.56 (kN/m^3) Unit weight of reinforced concrete=2400 (kg/m^3)=23.54 (kN/m^3) $(EA)_{adjusted} = [(EA)/(S_z)]$, $(EI)_{adjusted} = [(EI)/(S_z)]$								

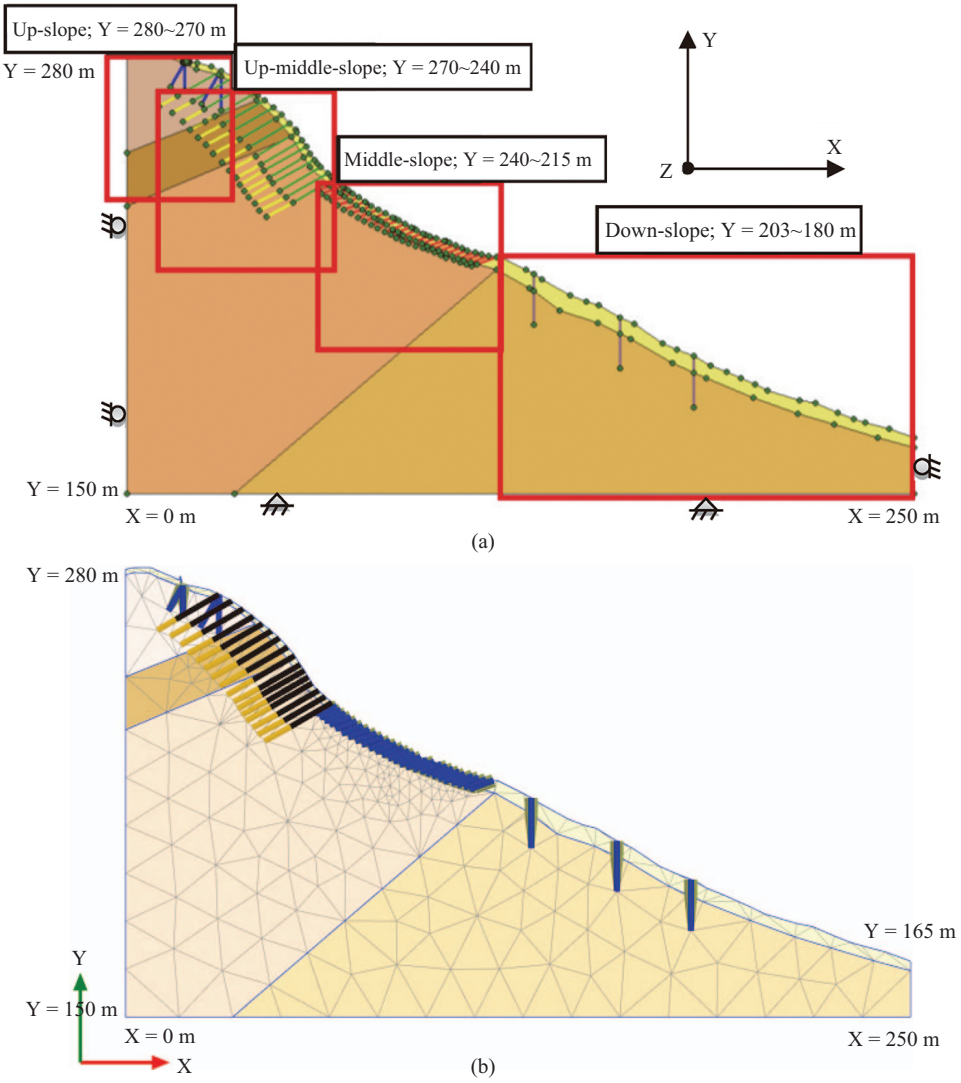

Fig. 12. (a) Numerical model (b) finite element mesh along C-C′ profile of T16-Slope after landslide with remediation of 4 sectional slopes.

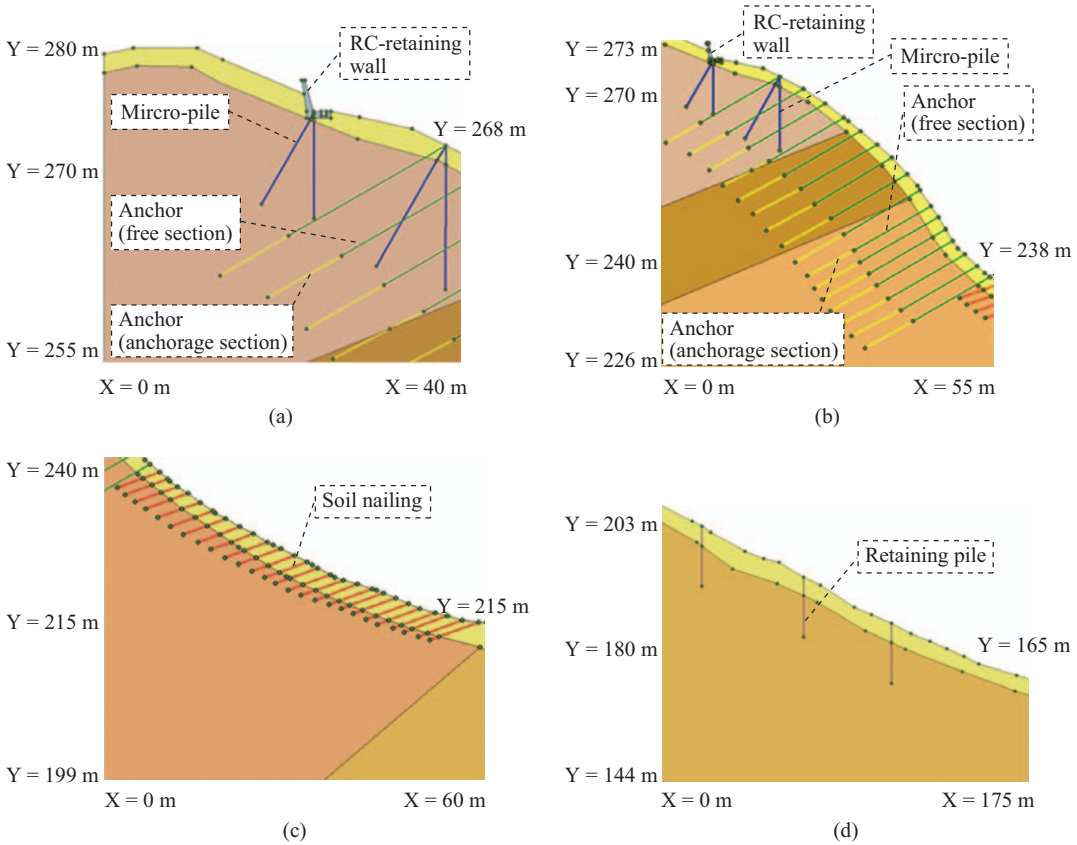

Fig. 13. Numerical model of sectional slopes subdivided from C-C′ profile of T16-Slope with remediation of (a) up-slope with micro-pile of steel rail and *RC*-retaining wall, Y = 280~270 m (b) up-middle-slope with RC-grid-beam and anchorage, Y = 270~240 m (3) middle-slope with *RC*-frame and soil nailing, Y = 240~215 m (4) down-slope with retaining piles, Y = 203~180 m (Y = elevation of remediation)

of safety with remediation, $(FS(t)_{with})$, for a rainfall duration of t, is compared with that without remediation, $(FS(t)_{without})$, and the effectiveness of remediation accomplished in *T16-Slope* is evaluated by a relative factor of safety, $RFS(t) = [(FS(t)_{with})/(FS(t)_{without})]$, which alternately used to quantify the contribution of remediation to the slope stability. However, it should be pointed out that the *SRM* can only reveal one *P*otential *S*liding *S*urface (*PSS*) for the stability analyses of entire *T16-Slope*. Meanwhile, the *PSS* possesses a minimum factor of safety and only develops at a certain sectional slope, (namely, up-slope, or up-middle-slope, or middle-slope, or down-slope) stabilized by a certain remediation method. As a consequence, although the stability analyses were performed for the entire *T16-Slope* with 4 remediation methods, as shown in Fig. 12, the stabilization effect can only be expressed for a certain remediation method corresponding to a certain sectional slope in terms of minimum factor of safety $FS(t)_{with}$ (also minimum factor safety of $FS(t)_{without}$ in Fig. 11) and the associated $RFS(t)$ value. In *SRM* stability analyses, the influence of mesh discretization or mesh coarseness on FS value is minor if the associated plasticity or associated flow rule is adopted (Tschuchnigg et al., 2015). In this study, the dilatancy angle of surficial colluviums is specified to be zero (Table 2) in *SRM* stability analyses and the reducing frictional angle in *SRM* calculation will never falls to the value of dilatancy angle. Consequently, the numerical instability with no clear indication of the failure mechanism (or indication of *PSS*) will not occur in the computation. In addition, the *PSS* mainly mobilizes in surficial colluviums with thin thickness and the mesh generation in this area becomes relatively dense when incorporating with the reinforcement. In such circumstances, a coarse mesh was eventually adopted for analyses.

6. Stability Analyses and Efficiency Evaluation for the Remediation of 4 Sectional Slopes

In order to evaluate the stabilization effect of individual remediation method, the numerical model of entire *T16-Slope* is subdivided into 4 sectional slopes from slope top to slope toe, as displayed in Figs. 13(a)-(d), for a series of slope stability analyses to investigate the locations of *PSS* and stabilization effects of different remediation methods for each individual section of the *T16-Slope*.

IV. RESULTS AND DISCUSSIONS

1. Stability Analyses of *T16-Slope* during Jang-Mi Typhoon

During Jang-Mi Typhoon (with rainfall duration $t = 77$ hours) for the initial stage of rainfall ($t = 0 \rightarrow 24$ hours) the Potential

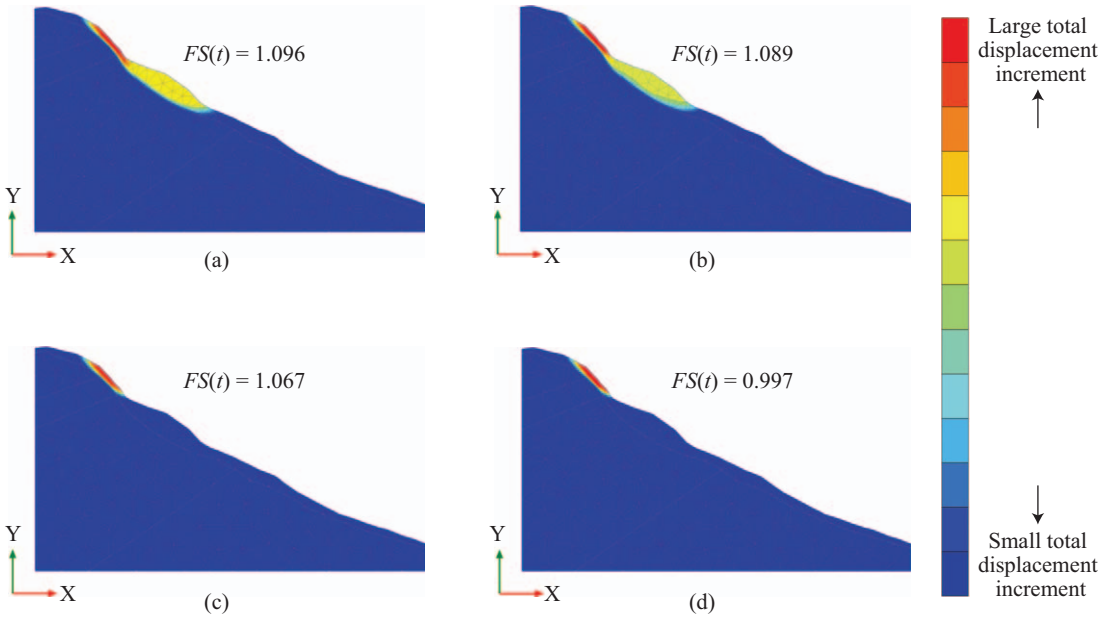

Fig. 14. Development of primary potential sliding zone of T16-Slope during Jang-Mi Typhoon (a) $t = 0$ hours (b) $t = 24$ hours (c) $t = 48$ hours (d) $t = 72$ hours.

Sliding Surface (*PSS*) of T16-Slope developed at the up-slope of red zone (primary *PSS* with steep gradient and larger total displacement increment) and yellow zone (secondary *PSS* with mild gradient and smaller total displacement increment), as shown in Figs. 14(a) and (b). The time-dependent factor of safety, $FS(t)$, tends to a lower value ($FS(t) = 1.096 \rightarrow 1.089$ for $t = 0 \rightarrow 24$ hours). Subsequently, the *PSS* gradually forms at the surficial colluviums of up-slope after the infiltration of rain-water at the later stage of rainfall ($t = 48 \rightarrow 72$ hours), as the red zone shown in Figs. 14(c) and (d), and the factor of safety of the *PSS* further descends and approaches a critical value of unity ($FS(t) = 1.067 \rightarrow 0.997 \approx 1.0$ for $t = 48 \rightarrow 72$ hours). Montrasio and Valentino (2008) indicated that rainfall-induced shallow landslides are usually triggered by intense rainfalls of short durations and it generally involves small portions of shallow soils and is characterized by high-density distributions over wide areas. As a result, it can be inferred that after the primary sliding of thin colluviums at up-slope (steep zone), the sliding can be transferred to the secondary sliding of thicker colluviums immediately below up-slope (mild zone). This simulation results coincide with the topographic variation of *T16-Slope* before (2006) and after (2008) the landslide as illustrated in Fig. 9.

The relationship of rainfall duration t ~ rainfall intensity I ~ factor of safety $FS(t)$ is illustrated in Fig. 15 and it indicates that the landslide of *T16-Slope* occurred in the rainfall duration of t = 64~72 hours when $FS(t)$ value approaches unity ($FS(t) \approx 1.0$). According to Fig. 15: (1) at the initial stage of rainfall ($t = 0 \sim 8$ hours), the $FS(t)$ values with minute increasing rate is resulted from the downward seepage force of infiltrated rainwater which alternately causes a slight consolidation effect (the factor of safety is calculated by an advanced mode of consolidation type) and an increase of effective stress of soil mass. However, the response of pore-water pressure is insignificant due to the lower rainfall intensity in the rainfall duration. (2) In the rainfall duration of t=8~16 hours, the $FS(t)$ values descend because of a highly raised rainfall intensity I accompanied with a large quantity of rainwater infiltration. (3) Subsequently, in the rainfall duration of t = 16~40 hours, although the rainfall intensity I raised gradually, the development and effect of excess pore-water pressure due to infiltrated rainwater are much lesser than the effect of infiltrated rainwater seeping toward the downslope. As a result, the $FS(t)$ values progressively pick up because of the increasing effective stress of soil mass due to seepage-induced consolidation effect. (4) After the rainfall duration of $t = 40$ hours, the rainfall sustains and maintains an intensity of certain level to accumulate a large quantity of rainwater. Consequently, the development and the effect of excess pore-water pressure resulted from infiltrated rainwater becomes predominant over the seepage-induced consolidation effect and the $FS(t)$ values continuously drops. (5) Finally, in

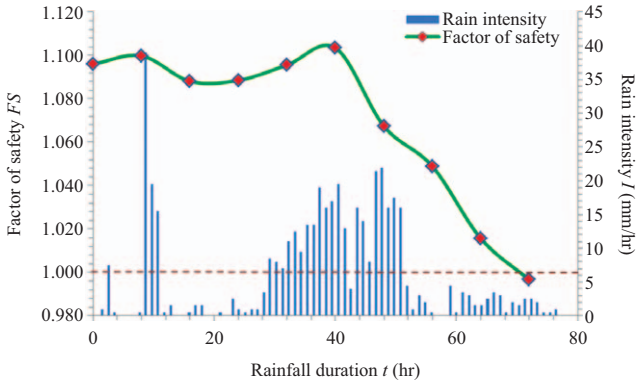

Fig. 15. Relationship of rainfall duration *t*~rainfall intensity *I*~factor of safety *FS*(*t*) of T16-Slope during Jang-Mi typhoon.

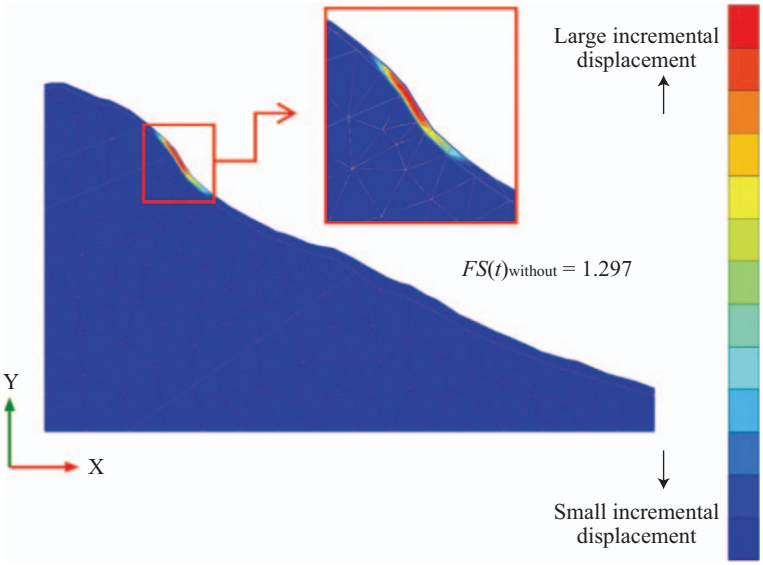

Fig. 16. Factor of safety $FS(t)_{without}$ = 1.297 (for t = 0 hours) and potential sliding surface of T16-Slope under dry condition after landslide without remediation.

the rainfall duration of t = 40~72 hours, the $FS(t)$ values descends continuously from 1.049 to 0.997 ($FS(t)$ = 1.049 → 0.997 for t = 40 → 72 hours) and this implies that the possible time for *T16-Slope* on the verge of failure is in the rainfall duration of t = 64~72 hours and coincides with the field observation of landslide occurring time at t = 64 hours (Fig. 3(b)). Comparatively, Sun et al. (2016) indicates that the variations of $FS(t)$ value for a *PSS* are consequently resulted from a combination of pore-air pressure, matric suction (negative pore-water pressure), and effective normal stress. However, the changes in pore-air pressure are usually ignored due to the difficulties in measuring the magnitude (Sako et al., 2011).

Based on the coincidence of comparisons between simulations and observations for the triggering mechanism and occurring time of landslide in *T16-Slope* during Jang-Mi typhoon, in addition to the verification of numerical procedures, one can calibrate the required material model parameters for rainfall-induced seepage and stability analyses as listed in Tables 2 and 3.

2. Stability Analyses of *T16-Slope* after Landslide without Remediation

The factor of safety of *T16-Slope* after landslide without remediation $(FS)_{without}$ = 1.297 (for t = 0 hours) under dry condition (Fig. 16) is higher than that before landslide $FS(t)_{t=0}$ = 1.096 (Fig. 14(a)) for 1.183 times. This is due to the fact that the topography of *T16-Slope* after landslide becomes milder than that before landslide and which alternately brings the slope into a more stable situation. Meanwhile, the *PSS* of *T16-Slope* after landslide remained at the steepest area of surficial colluviums (Fig. 16, red zone) and close to the primary potential sliding surface at the up-middle-slope of *T16-Slope* before landslide (Fig. 14(a), red zone).

A series of rainfall-induced seepage analyses are carried out using a 48-hour design rainfall of 5-, 10-, 25-, and 50-year return periods and only the numerical results of 25-year return period (Fig. 10(d)) are presented for an illustrative explanation. For the rainfall duration t = 0~24 hours, due to a lower rainfall intensity and insignificant rainwater infiltration, the corresponding factor of safety descends slightly from $FS(t)_{without}$ = 1.297 (for t = 0 hours) (Fig. 16) to $FS(t)_{without}$ = 1.239 (for t = 24 hours) (Fig. 17(a)). For the rainfall duration t = 0~24 hr, the increase of degree of saturation (S(%)) of unsaturated surficial colluviums is minor due to a lower rainfall intensity and insignificant rainwater infiltration (Fig. 17(c)). Subsequently, the factor of safety descends to $FS(t)_{without}$ = 1.045 (for t = 48 hours) and the *PSS* situates near the up-slope as shown in Fig. 17(b). For the rainfall duration t = 24~48 hr, the S (%) of unsaturated surficial colluviums ascends noticeably and approaches a saturated state for some surface areas of the slope at t = 48 hr as

Table 5. Factor of safety $FS(t)$ after of T16-Slope after landslide without remediation under a 48-hour design rainfall of different return periods.

Rainfall duration t (hours)	Return periods (year)	
	25	50
	$FS(t)_{without}$	
0	1.297	1.297
6	1.303	1.301
12	1.289	1.287
18	1.266	1.264
24	1.239	1.238
30	1.201	1.200
36	1.150	1.136
42	1.118	1.029
48	1.045	**1.004**

Table 6. Factor of safety FS(t)after of T16-Slope after landslide with remediation under a 48-hour design rainfall with 25-, 50- and 100-year return periods.

Rainfall duration t (hours)	Return periods (year)		
	25	50	100
	$FS(t)_{without}$		
0	1.659	1.659	1.659
6	1.605	1.605	1.602
12	1.575	1.572	1.570
18	1.573	1.536	1.532
24	1.466	1.440	1.435
30	1.376	1.366	1.362
36	1.317	1.309	1.305
42	1.282	1.238	1.237
48	1.242	**1.191**	1.174

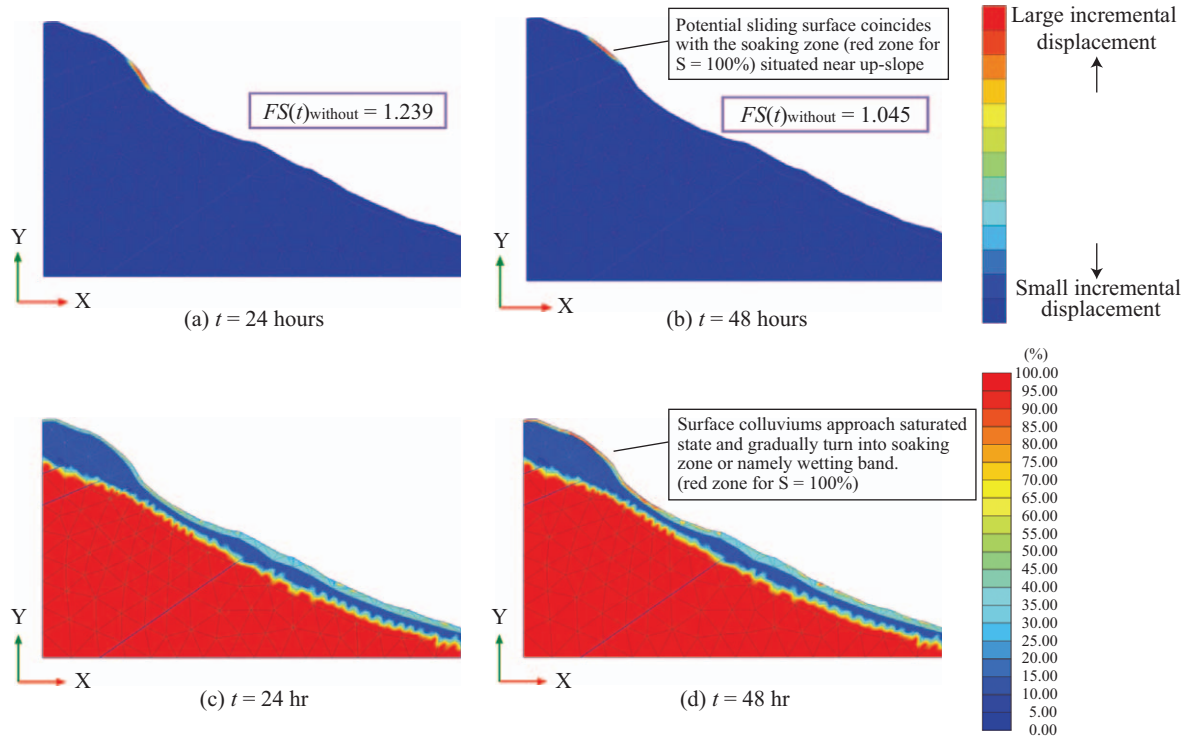

Fig. 17. The degree of saturation and potential sliding surface of T16-Slope under 48-hour design rainfall with 25-year return period after landslide without remediation (including the factor of safety $FS(t)_{without}$).

shown in Fig. 17(d). The *PSS* locates at the surficial colluviums with high degree of saturation area which gradually turns into a soaking zone (or wetting band) during rainfall. The shear resistance of soil mass in the soaking zone reduces and which leads to an unstable situation of the slope.

$FS(t)_{without}$ for 48-hour design rainfall with different return periods is summarized in Table 5 and only the numerical results without remediation for 25- and 50-year return periods are presented to compare with those with remediation (see Table 6). Numerical results indicate that for 50-year return period, the factor of safety largely descends from $FS(t)_{without} = 1.136$ to 1.004 (comes close to a critical state of $FS(t)_{without} = 1.0$) when the rainfall duration $t = 36$~48 hours is reached. Meanwhile, numerical results also reveal that the *T16-Slope* after landslide without remediation is unable to endure a full 48-hour design rainfall of 100-year return period and the slope failure occurs and the calculation ceases about at a rainfall duration $t = 24$ hours.

Negative pore water pressure, known as matric suction, provides an apparent cohesion that significantly increases the slope stability and also contributes additional shear strength to unsaturated soil slope. As water infiltrates into the slope, the decrease or loss of matric suction will cause the slope to be more susceptible to failure (Simon A. and Curini A., 1988; Rahardjo et al., 2012). In order to capture the variation of negative pore-water

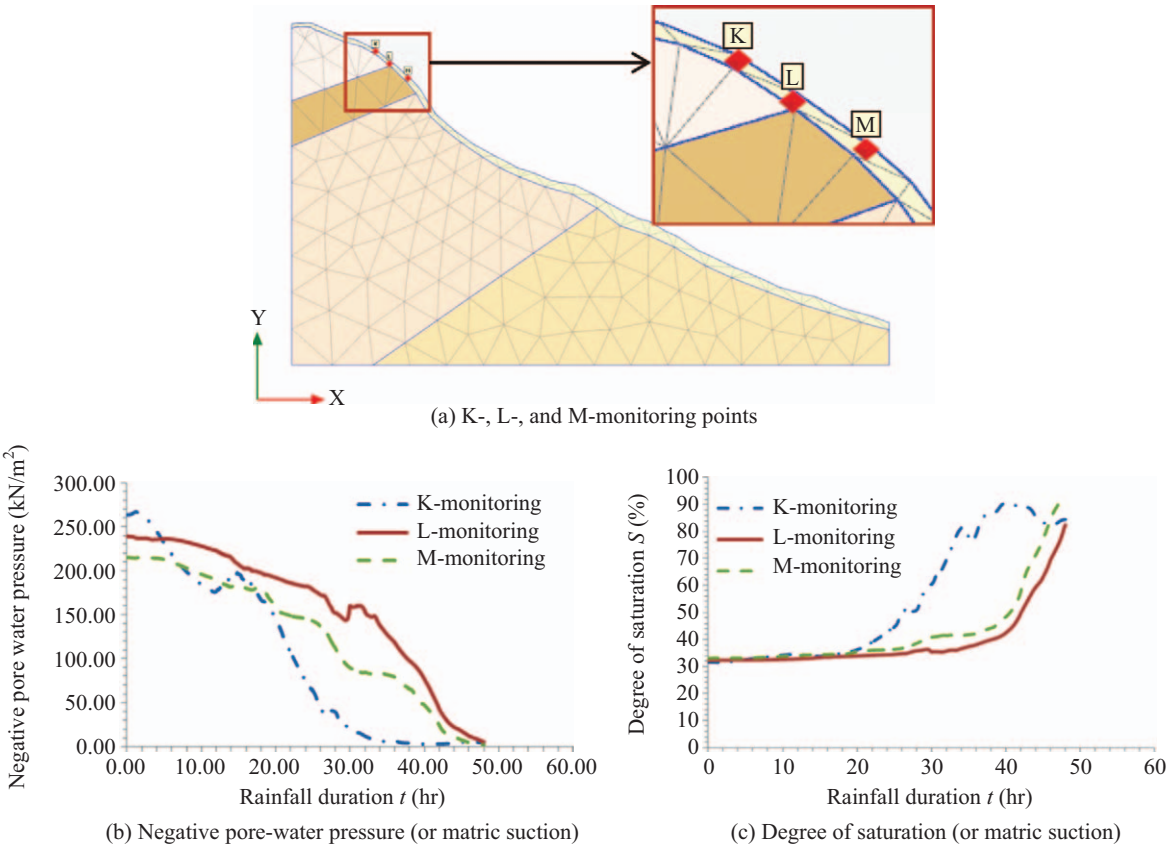

(a) K-, L-, and M-monitoring points

(b) Negative pore-water pressure (or matric suction)

(c) Degree of saturation (or matric suction)

Fig. 18. Variations of matric suction and degree saturation of unsaturated surficial colluviums of potential sliding zone under 48-hour design rainfall of 25-year return period after landslide without remediation.

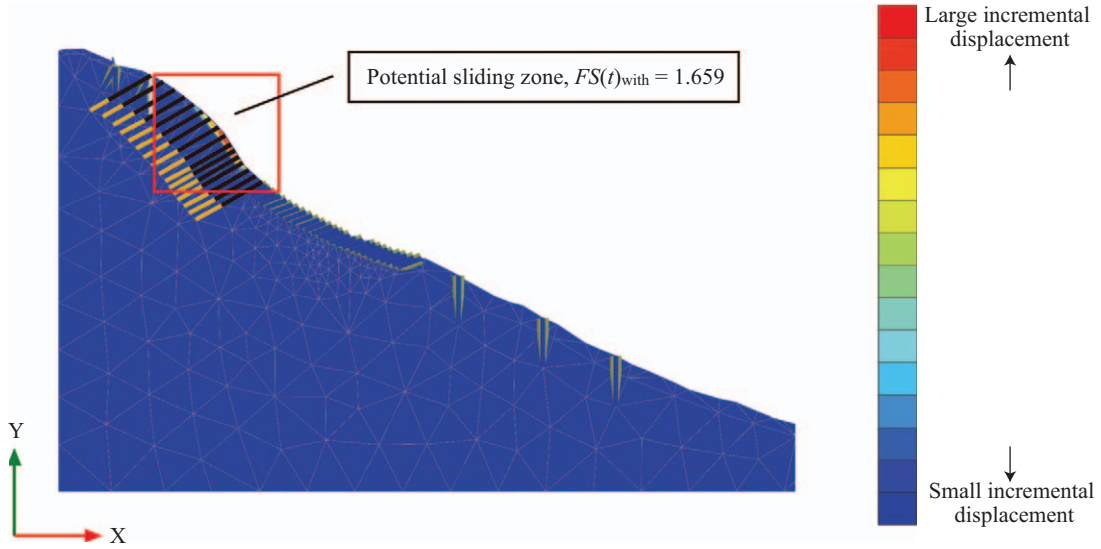

Fig. 19. Factor of safety $FS(t)_{with}$ (for t = 0 hours) and potential sliding zone of T16-Slope under dry condition with remediation

pressure u_w and degree of saturation S (%) of surficial colluviums of *T16-Slope* after landslide without remediation during rainfall, three monitoring points K (up-slope), L (middle-slope) and M (down-slope), as illustrated in Fig. 18(a), are set up along the *PSS* (Fig. 17(b)). The variation of u_w ($u_w < 0$) and S(%) of K-, L-, and M-point with rainwater infiltration during 48-hour design rainfall of 25-year return period is exhibited in Fig. 18(b) and (c). It can be observed that after 48 hours of rainfall the u_w values of three monitoring points nearly drop down to zero (matric suction losses) and the S(%) values increase to

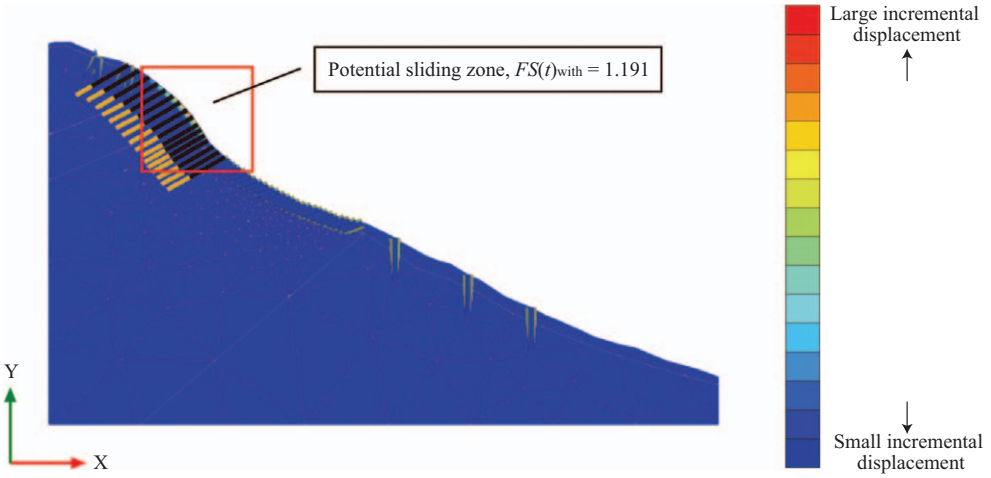

Fig. 20. Factor of safety $FS(t)_{with}$ (for t=48 hours) and potential sliding zone of T16-Slope under 48-hour design rainfall with return period of 50-year with remediation

80% (close to a saturated state). The above numerical results act in cooperation with several researches (Simon and Curini, 1998; Ng and Shi, 1998; Ng. et al., 2001; Cho and Lee, 2002; Rahardjo et al., 2007) which suggested that the failure mechanisms of the surficial layer during rainy seasons mainly involve rainfall-induced matric suction losses.

3. Overall Stability Analyses of *T16-Slope* with Remediation of 4 Sectional Slopes

After landslide, the overall stability of *T16-Slope* under dry condition with remediation made in 4 sectional slopes from the slope top to slope toe (Fig. 12) is displayed in Fig. 19. In which, the factor of safety $FS(t)_{without}$ = 1.297 (for t = 0 hours, Fig. 16) without remediation is promoted to $FS(t)_{with}$ = 1.659 (for t = 0 hours, Fig. 19) with remediation and it should be noted that both $FS(t)_{without}$ and $FS(t)_{with}$ are minima corresponding to their own *PSS* of entire *T16-Slope*. In addition, for the remediation of 4 sectional slopes from the slope top to slope toe of *T16-Slope*, the *PSS* mobilized at the up-middle-slope (Fig. 19) where a series of *RC*-grid-beam and anchorage was constructed is very close to that without remediation (Fig. 16). This demonstrates that after landslide the failure modes of *T16-Slope* for both cases with and without remediation are similar and the *PSS* for both cases is developed at the up-middle-slope.

The overall stability analyses of *T16-Slope* with remediation of 4 sectional slopes are carried out under 48-hour design rainfall of return periods with 25-, 50-, and 100-year. The potential sliding zone for a return period of 50-year is illustrated in Fig. 20 and the time-dependent factor of safety $FS(t)_{with}$ for different return periods is summarized in Table 6. As listed in the table, the factor of safety of *T16-Slope* with remediation descends to $FS(t)_{with}$ = 1.191 (for t = 48 hours) under a design rainfall of return period of 50-year and which is higher than that without remediation $FS(t)_{without}$ = 1.004 (Table 5) for 18.6 % (= [(1.191-1.004) × 100%]/1.004). This demonstrates that the remediation can effectively mitigate a fast deterioration of slope stability and prevent the slope from falling to a critical state condition during torrential rainfall ($FS(t)_{with}$ = 1.191 > 1.0). The remediation (*RC*-grid-beam and anchorage) made at the up-middle-slope becomes crucial to the slope stabilization. Nevertheless, it should be pointed out that the confining effect (or suppressing effect) and stabilized contribution of *RC*-grid-beam (or *RC*-grillage) on the slope surface are not considered in the numerical model and these might result in a lower and conservative $FS(t)_{with}$ values.

The relationship of *R*elative *F*actor of *S*afety *RFS*(t) (= $FS(t)_{with}$/$FS(t)_{without}$), rainfall duration t and rainfall intensity I (or *RFS*~t~I relationship) of *T16-Slope* after landslide with remediation of 4 sectional slopes under 48-hour design rainfall of return period of 50-year is illustrated in Fig. 21. At first, the remediation demonstrates a best stabilization effect on the slope at the initial dry condition without rainfall (t = 0 hours) and $FS(t)_{with}$ tends towards a highest value for a maximum *RFS* = 1.279. Subsequently, the *RFS* value descends to a minimum value ($RFS(t)_{min}$ = 1.145) at rainfall duration t = 30 hours and this is because of the slope just experienced a peak rainfall with intense infiltration of rainwater at t = 23~24 hours. The lowest value of *RFS* does not occur at the peak rainfall which reveals a lagging effect of infiltrated rainwater on the factor of safety. Eventually, the stabilization effects of remediation on the slope are gradually recovered with an ascending *RFS* value (or the $FS(t)_{with}$ tends to recover towards a higher value rather than $FS(t)_{without}$) due to a progressively descending rainfall intensity after rainfall duration t > 30 hours. The decrease of *RSF* (= $FS(t)_{with}/FS(t)_{without}$) value at the end of 48-hour rainfall can be caused by the increase of the rainfall intensity few hours (between 40 to 44 hours) before the 48th hour. Because of a lagging effect of infiltrated rainwater on the factor of safety, the drop of *RSF* occurs few hours later.

4. Individual Stability Analyses of 4 Sectional Slopes of *T16-Slope* without and with Remediation

After landslide, *T16-Slope* was renovated from slope top to slope toe for 4 sectional slopes. The numerical model of entire

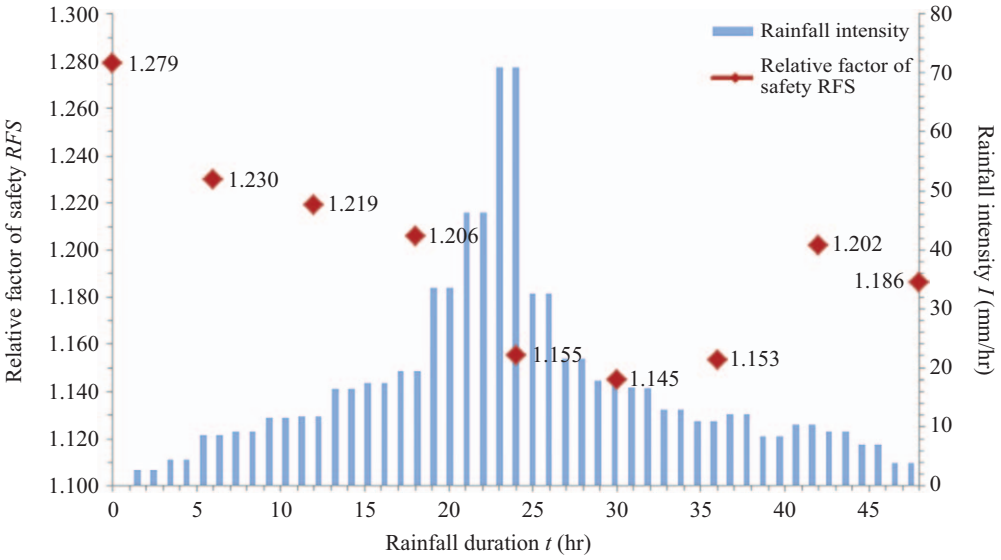

Fig. 21. *RFS~t~I* relationship of T16-Slope under 48-hour design rainfall with return period of 50-year after landslide with remediation.

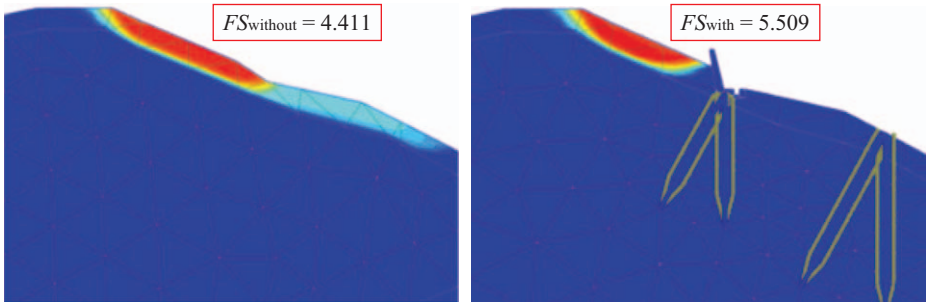

Fig. 22. The potential sliding surface and *FS* of up-slope (a) without (b) with micro-pile and *RC*-retaining wall.

T16-Slope partitioned into 4 sectional slopes can be referred to Fig. 13. The stability analyses of 4 sectional slopes under dry condition are shown in Figs. 22-25.

The factor of safety of up-slope is promoted by remediation (Fig. 22, $FS_{without}$ = 4.411 → FS_{with} = 5.509; $RFS = FS_{with}/FS_{without}$ = 1.249). Even though without remediation the up-slope remains in a comparatively stable condition due to possessing a fairly mild landform and high resistance of retaining structures. The construction of micro-pile and *RC*-retaining wall is aimed at securing the stability and safety of *T16*-tower pier immediately above the up-slope.

The stability of up-middle-slope is promoted by remediation (Fig. 23, $FS_{without}$ = 1.298 → FS_{with} = 1.661; $RFS = FS_{with}/FS_{without}$ = 1.280) and the *PSS* and *FS* values are very similar to those from the stability analyses of entire *T16-Slope* ($FS_{without}$ = 1.297 → FS_{with} = 1.659; Figs. 16 and 19). This implies that the up-middle-slope can be the most critical sectional slope for landslide in the future and more attention should be paid to the remediation. Repeatedly, it should be mentioned that the reinforcing and stabilizing effect of *RC*-grid-beam (or *RC*-grillage) on slope surface was not included in the numerical model.

The factor of safety of middle-slope *FS* is increased by remediation ($FS_{without}$ = 1.608 → FS_{with} = 2.029; $RFS = FS_{with}/FS_{without}$ = 1.585) for 58.5%. The *PSS* of middle-slope without remediation extends to a larger range of slope top (Fig. 24(a)) whereas is intercepted and restricted at a small area above the remediation (Fig. 24(b)). Similar to the up-middle-slope, the confinement effect and stabilization contribution of *RC*-frame on slope surface is not considered in the numerical model.

The factor of safety of down-slope *FS* is promoted by remediation ($FS_{without}$ = 1.670 → FS_{with} = 2.077; $RFS = FS_{with}/FS_{without}$ = 1.244). The analysis reveals that the *PSS* of down-slope without remediation spreads out to a large range from slope top to slope toe (Fig. 25(a)) but is captured in between two rows of retaining piles with remediation (Fig. 25(b)). Davies et al. (2003) indicated the design of pile spacing should maximize the amount of soil arching between the piles while minimizing the flow of soil between piles. It is generally considered that the flow between the piles is possible at pile spacing larger than 5 times of pile diameters *D* (Carder and Temporal, 2000). Moreover, based on the numerical results (Wei and Cheng, 2009 and 2010), the arching effect of surface soil strata between two

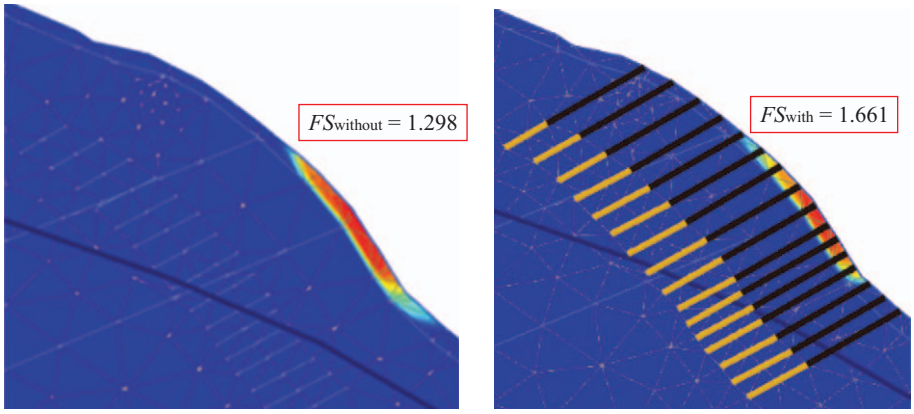

Fig. 23. The potential sliding surface and *FS* of up-middle-slope (a) without (b) with *RC*-grid-beam and anchorage.

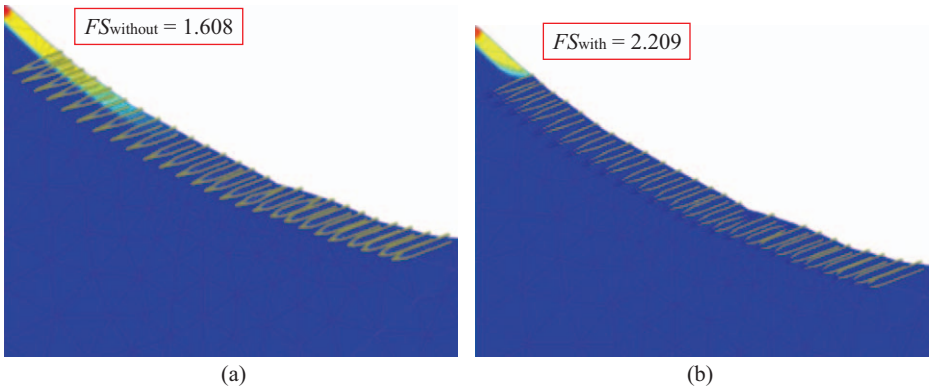

Fig. 24. The potential sliding surface and *FS* of middle-slope (a) without (b) with *RC*-frame and soil nailing.

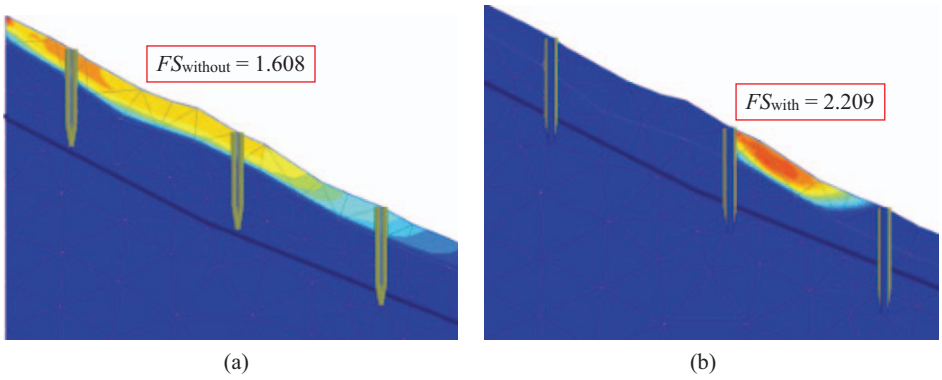

Fig. 25. The potential sliding surface and *FS* of down-slope (a) without (b) with retaining piles.

adjacent piles in *z*-direction can be mobilized to retain the downward flow of soil from upslope if the pile spacing smaller than $8 \times D$. In *T16-Slope*, the pile spacing $S_z = 1.2$ m is adopted for the pile design and which is much smaller than $5 \times D$~$8 \times D = 4.0$~6.4 m ($D = 0.8$ m). Although the arching effect of two adjacent piles in a row can be mobilized in practice, it is impossible for a plane strain analysis to reflect the arching effect in numerical model.

V. CONCLUSIONS

This study simulates the triggering mechanism of landslide of *T16-Slope* during the torrential rainfall of Jang-Mi typhoon. Meanwhile, after the landslide, the stabilization effects of remediation on *T16-Slope* are inspected under a 48-hour design rainfall of different return periods. According to the numerical results, several conclusions are made:

1. During the torrential rainfall of Jang-Mi typhoon, the location of sliding mass and occurrence time (or the initiation mechanism) of landslide (September, 28th, 2008) of simulation are coincided with those of observation based on the topographic variation of *T16-Slope* before (2006) and after (2008) landslide. To capture the initiation mechanism of landslide, it is indispensable to the numerical modeling to take the unsaturated behaviors of surficial colluviums into account in time-dependent rainfall-induced seepage and slope stability analyses.
2. To reflect the remediation effect of various engineering structures properly, the strength parameters of axial stiffness and flexural stiffness in 2-D plane strain analysis should be adjusted by considering the spacing effect.
3. The overall stability analyses of *T16-Slope* with remediation of 4 sectional slopes were carried out under 48-hour design rainfall of return periods of 50-year. The time-dependent factor of safety with remediation $FS(t)_{\text{with}} = 1.659$ descends to 1.191 (for $t = 0 \rightarrow 48$ hours) due to rainwater infiltration. However, the factor of safety with remediation $FS(t)_{\text{with}} = 1.191$ remains higher than that without remediation $FS(t)_{\text{without}} = 1.004$ for 18.6%. The remediation can effectively prevent the slope from fast deterioration and falling into a critical state condition ($FS(t)_{\text{with}} = 1.191 > 1.0$) during torrential rainfall.
4. Conclusively, because of a strenuous infiltration of rainwater resulted from a heavy intensity, the stabilization effects of remediation can be greatly reduced after a rainfall of long duration.
5. After landslide, *T16-Slope* is renovated from slope top to slope toe for 4 individual sectional slopes by different remediation methods. It is indicated that the up-middle-slope constantly exhibits a lowest stability (or lowest $FS(t)_{\text{without}}$ and $FS(t)_{\text{with}}$ values) without and with remediation. This also implies that the up-middle-slope can be the most critical sectional slope for the landslide in the future and more attention should be paid to the remediation.

REFERENCES

Berilgen, M. M. (2007). Investigation of stability of slopes under drawdown conditions. Computer Geotechnics 34, 81-91.

Bojorque, J., G. De Roeck and J. Maertens (2008). Comments on 'Two-dimensional slope stability analysis by limit equilibrium and strength reduction methods. Computer and Geotechnics 35, 305-308.

Carder, D. R. and J. Temporal (2000). A review of the use of spaced piles to stabilize embankment and cutting slopes. TRL report 466. TRL, Old Wokingham Road, Crowthorne, Berkshire, RG45 6AU, UK.

Chandrasekaran, S. S., R. Owaise Sayed, S. Ashwin, M. Jain Rayansh, S. Prasanth and R. B. Venugopalan (2013). Investigation on infrastructural damages by rainfall-induced landslides during November 2009 in Nilgiris, India. Journal of Natural Hazards 65, 1535-1557.

Cheng, Y. M., T. Lansivaara and W. B. Wei (2007). Two-dimensional slope stability analysis by limit equilibrium and strength reduction methods. Computer and Geotechnics 34, 137-150.

Cho, S. E. and S. R. Lee (2002). Evaluation of surficial stability for homogeneous slopes considering rainfall characteristics. Journal of Geotechnical and Geoenvironmental Engineering, 128:756-63.

Collins, B. D. and D. Znidarcic (2004). Stability analyses of rainfall induced landslides. J Geotech Geoenviron Eng130, 362-372.

Davies, J. P., F. A. Loveridge, J. Perry, D. Patterson and D. Carder (2003). Stabilization of a landslide on the M25 highway London's main artery. 12th Pan-American Conference on Soil Mechanics and Geotechnical Engineering, Boston, US, 22 - 25 Jun 2003.

Debray, S. and W. Z. Savage (2001). A preliminary finite-element analysis of a shallow landslide in the alki area of Seattle, Washington. Open-File Report 01-0357, U. S. Geological Survey.

Fredlund, D. G. and H. Rahardjo (1993). Soil Mechanics for Unsaturated Soils. John Wiley and Sons, Inc.

Fredlund, D. G. and N. R. Morgenstern (1997). Stress State Variables for Unsaturated Soils. Journal of Geotechnical Engineering Division, Proceedings, American Society of Civil Engineering (GTS) 103, 447-466.

Hoek, E. (2006). Practical Rock Engineering. e-book www.rocscience.com

Ko, S. Y. and D. G. Lin (2015). Rainfall-induced seepage and slope stability analyses. 2015 American Geophysical Union FALL MEETING, San Francisco, America, December 10-14, 2015, NH41C-1844.

Lin, D. G., B. S. Huang and S. H. Lin (2007). Quantitative evaluation on the stability of vegetated slope using the equivalent single taproot model. Journal of Chinese Soil Water Conserv. 38 (March (1)), 15-29. (in Chinese)

Lin, D. G., S. Y. Hsu, C. H. Chao, H. Y. Wen, S. M. Hsu, C. Y. Ku and S. Y. Chi (2008). Applications of simulation technique on hazard zone delineation and damage assessment of debris flow. Journal of Chinese Soil and Water Conservation 39 (4), 391-402. (in Chinese)

Lin, D. G., S. Y. Hsu and K. T. Chang (2009). Numerical simulations of flow motion and deposition characteristics of granular debris flows. Journal of Natural Hazards 50(3), 623-650.

Lin, D. G., Y. H. Lin and F. C. Yu (2010a). Numerical investigations of rainfall induced landslide. INTERPRAEVENT 2010 International Symposium in Pacific Rim, Taipei, Taiwan, April, 26-30, 528-541.

Lin, D. G., B. S. Huang and S. H. Lin (2010b). 3-D numerical investigations into the shear strength of the soil–root system of makino bamboo and its effect on slope stability. Journal of Ecological Engineering, Volume 36(8), 992-1006.

Lin, D. G., Y. H. Lin, C. Y. Wu and F. C. Yu (2012). An evaluation model of hazard potential for rainfall induced sediment-related slope disaster. Journal of Chinese Soil and Water Conservation 43(2),139-157. (in Chinese)

Montrasio, L. and R. Valentino (2008). A model for triggering mechanisms of shallow landslides. Nat Hazards Earth System Science 8, 1149-1159.

Ng, C. W. W. and Q. Shi (1998). A numerical investigation of the stability of unsaturated soil slopes subjected to transient seepage. Computers and Geotechnics 22(1), 1-28.

Ng, C. W. W., B. Wang and Y. K. Tung (2001). Three-dimensional numerical investigations of groundwater responses in an unsaturated slope subjected to various rainfall patterns. Canadian Geotechnical Journal 38, 1049-62.

O'Loughlin, C. and R. R. Ziemer (1982). The importance of root strength and deterioration rates upon EDAPHIC stability in steepland forests. In: I.U.F.R.O. Workshop P.1.07-00 Ecology of Subalpine Ecosystems as a Key to Management, 2-3 August, Corvallis Oregon, Oregon State University, 70-78.

Operstein, V. and S. Frydman (2002). The stability of soil slopes stabilised with vegetation. Ground Improv. 6, 163-168.

PLAXIS 2D (2015). Manual, website: www.plaxis.nl

Popescu, M. E. (2001). A suggested method for reporting landslide remedial measures. IAEG Bulletin, 60(1), 69-74.

Rahardjo, H., T. H. Ong, R. B. Rezaur and E. C. Leong (2007). Factors controlling instability of homogeneous soil slopes under rainfall. Journal of Geotechnical and Geoenvironmental Engineering 133(12), 1532-43.

Rahardjo, H., A. Satyanaga1 and E. C. Leong (2012). Unsaturated soil mechanics for slope stabilization. Geotechnical Engineering Journal of the SEAGS & AGSSEA 43(1), 48-58.

Sako, K., T. Danjo, R. Fukagawa and H. H. Bui (2011). Measurement of porewater and pore-air pressure in unsaturated soil. In: Proceeding of 5th Asia-Pacific Conference on Unsaturated Soils. Kasetsart University, Pattaya, 443-448.

Savage, W. Z., R. L. Baum, M. M. Morrissey and B. P. Arndt (2000). Finite-element analysis of the woodway landslide. Washington, U. S. Geological Survey Bulletin 2180, 1-9.

Simon, A. and A. Curini (1998). Pore pressure and bank stability: the influence

of matric suction. In: Hydraulic engineering '98. Memphis, TN: ASCE, Reston.

Singh, P. K., A. B. Wasnik,, A. Kainthola,, M. Sazid and T. N. Singh (2013). The stability of road cut cliff face along SH-121: a case study. Nat Hazards 68(2), 497–507.

Sun, D. M., X. M. Li,, F. Ping and Y. G. Zang (2016). Stability analysis of unsaturated soil slope during rainfall infiltration using coupled liquid-gas-solid three-phase model. Water Science and Engineering 9(3), 183-194.

Taipei City Government (2008). Evaluation report on the landslide of *T16-slope* at Royal Garden residential community, Wen-Shan district during Jang-Mi typhoon, Vols. 1 and 2.

Taipei City Government (2010). Technical report on design, construction and supervision of urgent remediation for the landslide of *T16-slope* during Jang-Mi typhoon.

Tsaparas, I., H. Rahardjo,, D. G. Toll and E. C. Leong (2002). Controlling parameters for rainfall-induced landslides. Computers and Geotechnics 29(1), 1-27.

van Genuchten, M. T. (1980). A closed-form equation for predicting the hydraulic conductivity of unsaturated soils. Soil Science Society of America Journal 44 (5), 892-898.

Tschuchnigg F., H. F. Schweiger and S.W. Sloan (2015). Slope stability analysis by means of finite element limit analysis and finite element strength reduction techniques. Part I: Numerical studies considering non-associated plasticity. Computer and Geotechnics 70, 169-177.

Wei, W. B., Y. M. Cheng and L. Li (2009). Three-dimensional slope failure analysis by the strength reduction and limit equilibrium methods. Computer and Geotechnics 36, 70-80.

Wei, W. B. and Y. M. Cheng (2009). Strength reduction analysis for slope reinforced by piles. Computers and Geotechnics 36(7), 1176-1185.

Wei, W. B. and Y. M. Cheng (2010). Soil nailed slope by strength reduction and limit equilibrium methods. Computers and Geotechnics 37(5), 602-618.

Wu, T. H., A. J. Watson and M. A. El-Khouly (2004). Soil-root interaction and slope stability ground and water bioengineering for erosion control and slope stabilization. Science Publisher, Inc., 183–192.

Zheng, Y. R. (2012). Development and application of the numerical limit analysis for geological materials. Chinese Journal of Rock Mechanics and Engineering 31(7), 1297-316. (in Chinese)